The Role of Atmospheric Noise in Decadal SST Variability

EDWIN K. SCHNEIDER,[a] BENJAMIN P. KIRTMAN,[b] AND NATALIE PERLIN[b]

[a] *George Mason University, Fairfax, Virginia*
[b] *Rosenstiel School of Marine and Atmospheric Science, University of Miami, Miami, Florida*

(Manuscript received 24 May 2022, in final form 6 December 2022)

ABSTRACT: A substantial role for atmospheric noise in simulations of decadal internal variability of SST is demonstrated by a comparison of a multicentury climate model control and a corresponding interactive ensemble (IE) simulation. The IE is designed to reduce atmospheric noise in the heat flux, wind stress, and freshwater flux at the air–sea interface. This comparison suggests that nearly all SST variability on decadal time scales is forced by internal atmospheric variability. The results are examined to determine the relative roles of atmospheric surface heat flux noise and ocean dynamics in the decadal volume-averaged heat budget of the upper ocean. The regional heat budgets in two regions, the South Pacific and the midlatitude North Atlantic, show the net atmospheric surface heat flux to be approximately in equilibrium with the ocean dynamics forcing. The IE and control results are used in the equilibrium heat budget approximation to infer the atmospheric heat flux response to SST, as well as the time series of the control atmospheric noise surface heat flux and ocean dynamics forcings for several regions. The South Pacific region SST is found to be primarily forced by the atmospheric noise surface heat flux and the North Atlantic region SST is forced by the ocean dynamics. Similar strengths for the atmospheric heat flux noise and ocean dynamics forcing, with an interdecadal atmospheric heat flux noise time scale and a centennial ocean dynamics time scale, are found for an Atlantic multidecadal variability region SST.

KEYWORDS: Fluxes; Atmosphere-ocean interaction; Sea surface temperature; Climate prediction; Interdecadal variability; Internal variability

1. Introduction

Understanding the mechanisms for decadal and longer time-scale climate variability in models can provide clues as to the predictability of the real climate system and how to efficiently realize that predictability (e.g., Keenlyside et al. 2008; Smith et al. 2012; Kirtman et al. 2013; Bombardi et al. 2015). The decadal variability problem is also important for attribution of climate variability to internal or external causes. This study is concerned with diagnosing the mechanisms for internal climate variability on decadal to centennial time scales (referred to in the following as "decadal") in a coupled general circulation model, with a focus on SST in the extratropical North Atlantic. Climate variability produced by external forcing, including changes in greenhouse gases other than water vapor, changes in the solar output or orbit, and changes in volcanic aerosol emissions, is not considered here. Candidate conceptual mechanisms for producing internal decadal climate variability of SST are internal variability of the oceans (not produced by atmospheric variability), forcing of the ocean by internal atmospheric variability (not produced by SST variability), and coupled atmosphere–ocean processes not involving intrinsic atmospheric or oceanic internal variability.

Hasselmann (1976) idealized atmospheric chaotic internal (weather) variability (Lorenz 1963) as a stochastic process (noise) forcing ocean heat storage and modeled coupled feedbacks as a linear damping of heat storage to demonstrate how the stochastic forcing by atmospheric surface heat flux alone could preferentially produce enhanced SST variability at long time scales in a process mathematically analogous to Brownian motion. The coupled feedback limits the response at low frequency and provides limited predictability due to persistence. The Hasselmann mechanism is a null hypothesis for internal climate variability. The major candidate to extend predictability beyond persistence is the inclusion of ocean dynamics. Hasselmann noted that statistical–dynamical models could be used to test the mechanism by adding stochastic forcing with statistical properties found from GCM numerical experiments or from meteorological data.

There has long been interest in the role of the Atlantic meridional overturning circulation (AMOC) on decadal SST variability. (e.g., Delworth et al. 1993; Dong and Sutton 2005; Danabasoglu et al. 2012; Ba et al. 2013; Meehl et al. 2014; Delworth and Zeng 2016; Kim et al. 2020). The AMOC heat transports can generate multidecadal SST variability in the North Atlantic Ocean, especially the Atlantic multidecadal variability (AMV) SST pattern, and respond to the atmospheric variability, especially the NAO (North Atlantic Oscillation). The main indicator of the effect of ocean dynamics, including the AMOC, on SST is the net surface heat flux at the ocean surface (taken as positive downward in the following). Gulev et al. (2013) noted strong negative correlations (order −0.5) between a decadally filtered AMV index (the average SST over approximately 30°–40°W, 40°–55°N) and the turbulent heat flux into the ocean. The sign of the correlation was reversed on interannual time scales. The conclusion was that these relationships demonstrate that ocean dynamics forcing of SST is strong at interdecadal time scales, while forcing from atmospheric surface heat flux predominates on interannual time scales. Clement et al. (2015) demonstrated that an atmospheric GCM coupled to a slab ocean model can

Corresponding author: Edwin K. Schneider, eschnei1@gmu.edu

DOI: 10.1175/JCLI-D-22-0399.1

© 2023 American Meteorological Society. For information regarding reuse of this content and general copyright information, consult the AMS Copyright Policy (www.ametsoc.org/PUBSReuseLicenses).

Brought to you by University of Maryland, McKeldin Library | Unauthenticated | Downloaded 08/23/24 06:34 PM UTC

generate multidecadal SST variability with the AMV pattern and amplitude resembling observations. This model configuration eliminates the effects of oceanic motions as in the original Hasselmann formulation, so that the forcing of local SST variability is only by local atmospheric surface heat fluxes. The results call into question the role of ocean dynamics in AMV. Clement et al. (2015) stimulated several studies arguing for the importance of ocean dynamics forcing of AMV (Zhang et al. 2016; O'Reilly et al. 2016; Delworth et al. 2017; Kim et al. 2018). In response, Clement et al. (2016) and Cane et al. (2017) generated examples using a simple single point model of the decadally filtered surface layer heat budget. In this model, white noise atmospheric noise surface heat flux and oceanic dynamics forcings are balanced by damping of SST resulting from the atmospheric heat flux response to the SST anomalies. Heat content variability is small relative to the forcing terms, so that the total atmospheric heat content tendency (the sum of the atmospheric heat flux noise forcing and the response to the SST) and the oceanic heat content tendency are equal and opposite. This model demonstrates gaps in the correlation and lag regression arguments made in some of the above studies. In particular, the decadal time filtering that removes the short time-scale variability also leads to spreading of the lag regressions to longer time scales. Additionally, adding even a relatively small oceanic contribution relative to the atmospheric forcing can lead to a substantial negative correlation between surface heat flux and SST in the special case when the atmospheric and ocean dynamics forcings are uncorrelated. However, Cane et al. (2017) note that their examples do not preclude a major role for ocean dynamics, only that more evidence is needed to make a convincing case for its importance. Zhang (2017) suggested that damping of SST by oceanic processes should be explicitly included in the simple model. This would create a threshold that the magnitude of stochastic ocean forcing would have to exceed in order to produce the negative heat flux/SST correlation. Liu et al. (2023) applied the Zhang (2017) simple model formulation using data from a climate model simulation and also using observational data, and found in both cases that the oceanic dynamics (defined as the part of the ocean tendency not including the ocean SST damping) is comparable to atmospheric noise forcing on decadal time scales.

Several CGCM (coupled GCM)-based studies have been carried out by our group to test a generalized version the Hasselmann mechanism, including all forms of atmospheric noise surface flux forcing of the ocean and its motions, (i.e., heat, wind stress, and freshwater), and their implications in the context of state-of-the-art (at the time of the numerical experiments) climate models (Wu et al. 2004; Schneider and Fan 2007; Kirtman et al. 2009, 2011; Fan and Schneider 2012; Chen et al. 2013, 2016; Kirtman et al. 2017; Zhang and Kirtman 2019; Colfescu and Schneider 2020). These studies have used interactive ensemble (IE) versions of various CGCMs (Kirtman and Shukla 2002) as statistical–dynamical models in the manner suggested by Hasselmann. An IE CGCM has, in principle, the same coupled feedbacks between the atmosphere and ocean as the standard version of the CGCM, since the dynamics and physics of the IE are the same as in the standard version. However, the atmospheric noise forcing of the ocean in the IE is small compared to that in the standard version. Chen et al. (2016) applied specified noise surface flux forcing inferred from a multicentury CGCM simulation to 100-yr simulations with the IE version of the CGCM, and demonstrated that atmospheric heat flux noise explained most of the multidecadal AMV in the eastern North Atlantic. The multidecadal AMV between 40° and 50°N in the central and western North Atlantic was the response to the wind stress noise. While substantial AMOC variability in the IE was forced by specifying the heat flux noise or wind stress noise alone, the AMOC variability associated with the AMV appeared to be primarily the response to the wind stress noise. On the other hand, Colfescu and Schneider (2020) found that forcing an IE by atmospheric noise was insufficient to explain internal decadal AMV variability in the subpolar gyre in a 130-yr historical CGCM simulation. However, this result was highly uncertain due issues involving the removal of the externally forced signal and the climate drift produced by initialization of the IE.

There are two scientific objectives of this paper. The first is to test a generalized version of the Hasselmann null hypothesis, by determining to what extent forcing by the atmospheric noise, as transmitted to the ocean by the noise in the surface heat flux, wind stress, and freshwater flux, is responsible for decadal SST variability in the CGCM. The second objective is to determine of the role of the dynamical ocean model as opposed to that of a one-dimensional slab ocean model in the decadal SST variability, including AMV, in the CGCM.

Section 2 summarizes the CGCM (CCSM4 Community Climate System Model, Version 4) and the IE version of CCSM4. The influence of revisions in the IE coupling on biases in the IE simulation relative to that of the CGCM are reported. Diagnostic methods for the heat budget analysis and the evaluation of the variance of the atmospheric heat flux noise are described.

Section 3 presents some updated results concerning the first objective, from the basic experiment comparing the IE and CCSM4, demonstrating the predominant role of the combined effect of all forms of atmospheric surface flux noise in forcing the decadal SST and AMOC variability. The balance of terms in the decadally filtered heat budgets integrated over the upper ocean are compared for two regions, one in the South Pacific and one in the midlatitude North Atlantic. The heat budgets in both regions are found to be a near-equilibrium between the total atmospheric heat flux and the ocean dynamics contributions, but little is found from the budget approach to indicate the role of the atmospheric noise in either contribution. The IE atmospheric component ensemble is used to estimate the ratio of the atmospheric heat flux noise variance to that of the total atmospheric heat flux in the CGCM simulation.

Section 4 focuses on the second objective through determining the relative importance of the atmospheric heat flux noise and ocean dynamics terms in the heat budget of the decadal SST variability of the CGCM simulation, as in earlier studies. Using results described in section 3 and a local linear approximation of the atmospheric heat flux response to SST,

Brought to you by University of Maryland, McKeldin Library | Unauthenticated | Downloaded 08/23/24 06:34 PM UTC

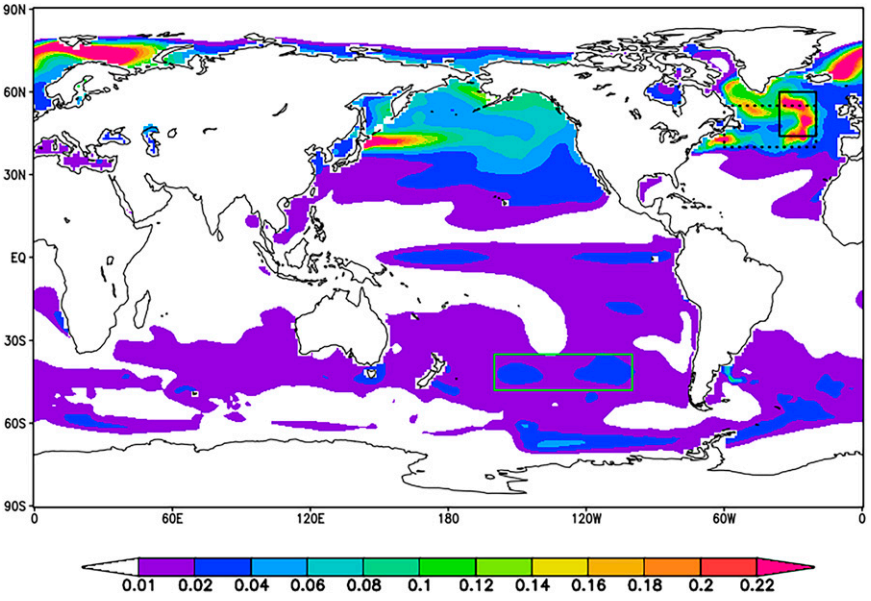

FIG. 1. Variance of detrended 9-yr running mean CONTROL SST (K^2). The NNA region is indicated by the solid black box, the SPA region is indicated by the green box, and the AMV_{mid} region is indicated by the dotted black box.

solutions are obtained in the two regions considered in section 3 as well as for an AMV region. The solutions include the strength of the atmospheric feedback to SST and the time dependent atmospheric heat flux noise and ocean dynamics contributions. The atmospheric and oceanic forcings are expressed as SST indices and used in a regression analysis, producing maps of the contributions of the atmospheric and oceanic forcing in the CGCM.

2. Models, simulations, and analysis

a. CGCM CONTROL

Aspects of the models and simulations analyzed here have been described by Kirtman et al. (2017) and Zhang and Kirtman (2019). The baseline model is the CCSM4 CGCM (Gent et al. 2011, equivalent to the CESM1.0 CGCM). The resolution of the atmospheric component, CAM4, the same atmospheric component used in the Clement et al. (2015) slab ocean runs, is approximately 1° in the horizontal with 26 vertical levels. The resolution of the ocean component, POP2, is approximately 1° in the horizontal with 60 vertical levels. Other component models include land and sea ice. A 500-yr CCSM4 simulation, denoted CONTROL uses 1990 external forcing.

Results presented here, referred to as "decadal," are 9-yr running means to filter out the subdecadal variability (Zhang and Kirtman 2019). The variance of the detrended CONTROL decadal SST, with the running means centered on years 205–496, is shown in Fig. 1. The variance is strongest in the Northern Hemisphere 30°–75°N. There are some other regions with locally enhanced variance, but much weaker than that in the Northern Hemisphere, including the equatorial Pacific and the midlatitude South Pacific. The analysis below will focus on determining the mechanisms for this enhanced variability, especially the roles of atmospheric noise forcing and ocean dynamics, in two of these regions: SPA, the region inside the green box in the South Pacific, and NNA, the northern North Atlantic region inside the black box. These regions are chosen primary to illustrate the role of the atmospheric noise in different regimes. The Cane et al. (2017) diagnosis is extended to evaluate of the relative roles of ocean dynamics and atmospheric surface heat flux noise in these two regions as well as in the AMV_{mid} region, shown by the dotted black box intersecting the NNA box.

b. The interactive ensemble version of the baseline model

The diagnostic model, IE-CCSM4, is an interactive ensemble CGCM version of CCSM4. A 500-yr simulation of IE-CCSM4 with 1990 external forcing, denoted IE, was carried out to isolate the role of forcing of ocean variability by internal atmospheric noise. The IE coupling strategy was first described in Kirtman and Shukla (2002). The atmospheric noise forcing of the ocean is reduced by coupling the ocean to an ensemble of atmospheric components instead of a single atmosphere as in CCSM4. Each atmospheric component sees the same SST from the ocean component, but is started with different initial conditions, and therefore has a different noise evolution. The noise in each atmospheric component has the same statistical properties, and similar statistical properties to the noise in the CGCM atmosphere. The ocean receives the ensemble mean of the surface fluxes from the atmospheric ensemble, thus reducing the noise in the forcing of the ocean.

IE-CCSM4 is constructed from the same component models at the same resolutions as in CCSM4. The IE atmospheric component is a 10-member ensemble of CAM4 atmospheres. The number of ensemble members was the largest that was practical,

Brought to you by University of Maryland, McKeldin Library | Unauthenticated | Downloaded 08/23/24 06:34 PM UTC

balancing the multicentury length of the IE simulation, the resolutions desired for the component models, and the available computational resources. It would be desirable to have the flexibility to employ objective error criteria (e.g., Milinski et al. 2020) in the design of future IE experiments. The surface fluxes provided by the atmosphere to the ocean (i.e., heat, wind stress, and freshwater) are the ensemble means of the surface fluxes of the IE atmospheric ensemble members. Since the atmospheric ensemble members start with different initial conditions and each member sees the same SST, the noise in the ensemble mean surface flux has 1/(number of atmospheric ensemble members) = 1/10 the variance of the noise in a single atmospheric component (Wu et al. 2004). Additionally, each atmospheric ensemble member is coupled to a separate land model and a separate sea ice model, 10 land models and 10 sea ice models in all. The fluxes from land to ocean (e.g., freshwater from runoff) and from sea ice to ocean (heat, stress, and freshwater) are also computed as ensemble means from the land and sea ice ensembles.

This configuration for land and sea ice components differs from that of IE-CCSM3, which was constructed from a previous version of the CCSM3 CGCM (Kirtman et al. 2009). In the IE-CCSM3, there was a single land component and a single sea ice component, each coupled to the atmospheric ensemble through the ensemble mean atmospheric prognostic surface fields (winds, humidity, temperature, precipitation). In both CCSM3 and CCSM4 and their IE versions there is full atmosphere–land and atmosphere–sea ice coupling, with updating of instantaneous surface model and atmospheric fields occurring together every time step (many times per day). On the other hand, the ocean temperature is updated only once daily from the diurnal mean of the surface fluxes computed every time step in the atmospheric component.

The use of ensemble mean atmospheric fields in updating the land and sea ice models led to serious biases over continental-scale areas in the IE annual mean surface temperature in IE-CCSM3 relative to CCSM3, with midlatitude land more than 2°C too cold and high latitude land in the Northern Hemisphere systematically more than 3°C too warm (Kirtman et al. 2011, their Fig. 1). The coupling of a land and a sea ice component to each atmosphere in IE-CCSM4 as in a traditional AMIP ensemble restores the noise forcing of the individual land and sea ice components and leads to much closer agreement between the IE-CCSM4 and CCSM4 climatological surface temperatures (obtained as ensemble means from the atmospheric model ensemble members) except in high latitudes (Fig. 2a). The IE-CCSM4 biases are reduced relative to CCSM4, but at the expense of eliminating the noise reduction from the IE coupling over land and sea ice, since each land and sea ice model responds to different atmospheric forcing. The cold biases near the Kamchatka Peninsula and in the midlatitude North Atlantic are found in both IE-CCSM4 and IE-CCSM3, while the cold bias in the Labrador Sea and Baffin Bay in IE-CCSM4 is a region of warm bias in IE-CCSM3. Large biases in high latitudes in IE-CCSM4, positive in the Arctic and negative near Antarctica, were also present with the same sign in IE-CCSM3. The cause remains to be found.

A related bias in IE-CCSM3 is a weak AMOC compared to the parent CGCM, CCSM3. The strength of the climatological

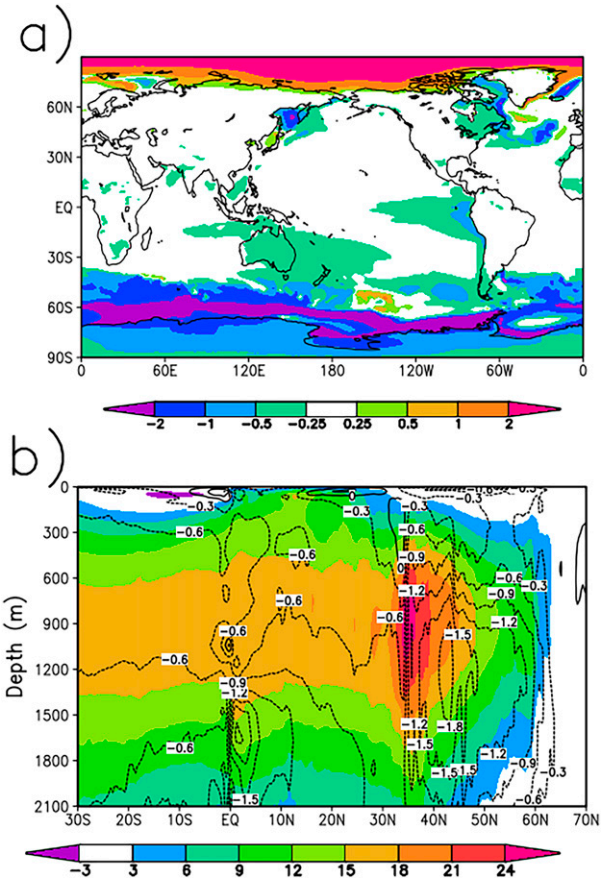

FIG. 2. (a) Climatological surface temperature bias (°C) averaged over years 201–500 in IE-CCSM4 compared to CONTROL. (b) AMOC streamfunction (Sv) averaged over years 201–500 for CONTROL (shaded) and IE bias (contours; interval 0.3 Sv).

AMOC is 22 Sv (1 Sv $\equiv 10^6$ m^3 s^{-1}) in CCSM3, but only 17 Sv in IE-CCSM3. This bias has been reduced in IE-CCSM4 compared to CCSM4 (Fig. 2b), apparently an impact of the smaller land surface temperature biases on the ocean. The climatological AMOC strength averaged over years 201–500 of CONTROL is about 25 Sv. The IE-CCSM4 AMOC is about 1.5 Sv weaker in IE, less than half of the bias in IE-CCSM3. The IE bias of a shallow counterclockwise closed cell with a strength of −0.5 Sv in the top 100 m of the midlatitude North Atlantic may be related to the cold SST bias in that region through reduced poleward transport of the warmer surface waters.

c. *Volume-integrated ocean heat budget*

The volume-integrated ocean heat budget with the climatological mean and annual cycle removed is calculated to help understand the mechanisms of the decadal SST variability. The approach is similar to that used in Buckley et al. (2014). The components of the heat budget are integrated over a vertical column extending from the ocean surface to depth d, taken as 100 m, in order to document the roles of atmospheric net surface heat fluxes and upper ocean dynamics in the SST variability. The 100-m depth of the layer is chosen to be below

Brought to you by University of Maryland, McKeldin Library | Unauthenticated | Downloaded 08/23/24 06:34 PM UTC

the levels of strongest vertical mixing and to represent a layer of the ocean that is strongly related to the SST variability. The dependence of the heat budget results on this choice is described below. The volume-integrated ocean heat budget is straightforward to derive and is written as

$$\frac{dH}{dt} = Q_a + Q_O. \tag{1a}$$

The term dH/dt represents the anomalous heat storage in the volume. The term Q_a is the net surface heat flux from the atmosphere into the volume, while Q_O is the volume-integrated ocean dynamics tendency. While Q_O can result in part from atmospheric heat flux forcing (e.g., Chen et al. 2016), these contributions are considered here as forcing by ocean dynamics. The heat storage is computed as the tendency of H, where H is the volume integral of the heat content $h = \rho cT$, where T is the temperature, ρ is the water density, and c is the specific heat of water. The ocean dynamics tendency is found from

$$Q_O = D + U, \tag{1b}$$

where D is the resolved ocean dynamics tendency and U is the unresolved ocean dynamics tendency. The resolved ocean dynamics tendency $D = -\langle \nabla \cdot (\mathbf{v}h) \rangle = -\langle (\partial/\partial x)(uh) + (\partial/\partial y)(vh) + (\partial/\partial z)(wh) \rangle$, where the angle brackets denote the volume integral, is computed from the monthly means of both h and the full velocity, $\mathbf{v} = (u, v, w)$ The term U is found as the residual necessary for [(1a) and (1b)] to be satisfied. It is "unresolved" since the model diagnostics required to calculate it explicitly were not included in the model output. The unresolved ocean dynamics tendency is due to motions on shorter than monthly time scales as well as to the model parameterizations of various types of mixing.

The contribution D_{ek} to the resolved ocean dynamics tendency from the monthly Ekman velocity $\mathbf{v}_{\mathrm{ek}} = (u_{\mathrm{ek}}, v_{\mathrm{ek}}, w_{\mathrm{ek}})$ response to the surface wind stress $\boldsymbol{\tau} = (\tau_x, \tau_y)$ is also estimated. Integrating the balanced ageostrophic momentum budget (Coriolis + friction = 0) from $-d$ to the surface with $u_{\mathrm{ek}}|_{z=-d} = v_{\mathrm{ek}}|_{z=-d} = w_{\mathrm{ek}}|_{z=0} = 0$, the vertical mean horizontal Ekman velocities and the vertical Ekman velocity at $-d$ are

$$v_{\mathrm{ek}} = -\frac{\tau_x}{\rho f d}, \; u_{\mathrm{ek}} = \frac{\tau_y}{\rho f d}, \; w_{\mathrm{ek}}|_{z=-d} = \frac{\nabla \times \boldsymbol{\tau}}{\rho f}, \tag{2}$$

with f taken as the average value of the Coriolis parameter over the region under consideration. The heat content tendency from the resolved Ekman heat transports is then found from

$$D_{\mathrm{ek}} = -\langle \nabla \cdot (\mathbf{v}_{\mathrm{ek}} h) \rangle = -\left\langle \frac{\partial}{\partial x}(u_{\mathrm{ek}} h) + \frac{\partial}{\partial y}(v_{\mathrm{ek}} h) + \frac{\partial}{\partial z}(h \tilde{w}_{\mathrm{ek}}) \right\rangle, \tag{3}$$

where $\tilde{w}_{\mathrm{ek}}|_{z=0} = 0$ and $\tilde{w}_{\mathrm{ek}}|_{z<0} = w_{\mathrm{ek}}|_{z=-d}$ for convenience, since the vertical integral of the third term on the rhs of (3) depends only on the values of $\tilde{w}_{\mathrm{ek}}$ at $z = 0$ and $z = -d$.

The heat budget analysis is applied to the model output from both CONTROL and IE. The annual means of T, $\nabla \cdot (\mathbf{v}T)$, and Q_a are calculated from the monthly values at each point on the ocean model grid and saved. The monthly heat flux divergence calculations use the monthly means of $\mathbf{v}$ and T and the ocean model's spatial differencing formulation. The saved annual values are used to find the annual mean volume or area integrals of the terms in [(1a) and (1b)] for the various regions. Climatological means are removed, 9-yr running means of the volume-integrated terms filter out subdecadal variability, and the terms are detrended.

d. *Atmospheric heat flux noise variance estimate for CONTROL*

An estimate of the variance of the heat flux noise in CONTROL will be used in section 3c. However, the experimental design does not provide the CONTROL noise directly. Deser et al. (2012) used a 10 000-yr CAM3 AGCM simulation forced by an observation-based climatological SST with repeating annual cycle to produce plausible estimates of the properties of atmospheric internal variability. CAM3 is the atmospheric component of the CCSM3 CGCM, the predecessor to the CCSM4 CGCM used in this study.

Here, the CONTROL decadal heat flux noise variance is estimated to be the average of the variances of the 9-yr running means of the heat flux noise in the individual members of the IE atmospheric model ensemble. The justification follows. The total net surface heat flux Q_a^C in CONTROL or $Q_a^{\mathrm{IE}_i}$ in member i of the M-member IE atmospheric model ensemble is composed of the response of the atmospheric model to the SST variability, F_C or F_{IE}^i, and noise, N_C or N_{IE}^i:

$$Q_a^C = F_C + N_C, \tag{4a}$$

$$Q_a^{\mathrm{IE}_i} = F_{\mathrm{IE}}^i + N_{\mathrm{IE}}^i. \tag{4b}$$

Since each of the members of the IE atmospheric model ensemble has the same time dependent SST lower boundary condition, the response F_{IE}^i in (4b) is the same for each member, $F_{\mathrm{IE}}^i = F_{\mathrm{IE}}$. The responses F_C and F_{IE} differ since the CONTROL and IE SST evolutions are different. The IE ensemble members are assumed to have different uncorrelated samples of noise N_{IE}^i from a population with variance $\mathrm{Var}(N_{\mathrm{IE}})$. Then taking the ensemble mean of (4b), the SST forced response in the IE is approximately the ensemble mean of the $Q_a^{\mathrm{IE}_i}$:

$$F_{\mathrm{IE}} \approx \frac{1}{M} \sum_{i=1}^{M} Q_a^{\mathrm{IE}_i}$$

and the approximate noise evolution of member i is given by

$$N_{\mathrm{IE}}^i \approx Q_a^{\mathrm{IE}_i} - F_{\mathrm{IE}}.$$

The atmospheric response to the SST contains contributions from both local and remote SST variability. Since the variance of the SST anomalies, and hence the response, in IE turns out to be small compared to that in CONTROL as shown below, the variance of the SST forced response in an IE atmospheric ensemble member is much smaller than that in CONTROL,

Brought to you by University of Maryland, McKeldin Library | Unauthenticated | Downloaded 08/23/24 06:34 PM UTC

$\mathrm{Var}(F_{\mathrm{IE}}) \ll \mathrm{Var}(F_C)$ and close to the $F_{\mathrm{IE}} = 0$ case of forcing by the annually varying climatological SST (e.g., Deser et al. 2012). The estimated noise variance in CONTROL is taken to be the same as the unbiased mean variance [Chen et al.'s (2013) online supplemental material] of the variances of the IE atmospheric model ensemble members, effectively assuming that the noise variance in the atmospheric component of CONTROL is independent of the SST anomalies:

$$\mathrm{Var}(N_C) \approx \mathrm{Var}(N_{\mathrm{IE}}) = \frac{1}{M-1}\sum_{i=1}^{M}\mathrm{Var}(N_{\mathrm{IE}}^{i}). \qquad (5)$$

The same procedure is applied to the zonal wind stress to estimate the variance of the zonal wind stress noise.

A more accurate estimate of the noise could be obtained, and the assumption that the noise does not depend on the SST anomalies could be verified, if the atmospheric response to the actual SST anomalies of CONTROL was included. The CONTROL SST forced response could be calculated from an AMIP ensemble (Gates et al. 1999) forced by the time evolving SST of CONTROL, as in Fan and Schneider (2012), Chen et al. (2013), and Colfescu and Schneider (2017); however, these atmospheric model runs have not been conducted for this model.

3. Results from simulations

a. *Decadal SST forcing by the atmospheric noise in CONTROL and IE*

Figure 3a shows the IE to CONTROL decadal variance ratios for the detrended 9-yr running means of years 201–500 annual mean SST (cf. Fig. 2f of Zhang and Kirtman 2019). Since the ensemble mean of the surface fluxes in an M-component IE atmospheric ensemble filters the variance of each component of the atmospheric noise forcing the ocean to be about $1/M$ of that in a single atmospheric component, the SST variance ratio should be 1/10 if all SST variability in CONTROL and the IE (with $M = 10$) is forced by the atmospheric noise (Wu et al. 2004).

A new element of the analysis here compared to earlier IE studies is statistical testing for whether IE variances are different from the expected noise forced value. The significance levels of the differences of the ratios from the noise-forced ratio of 0.1 are shown in Fig. 3b. The ratios, either larger or smaller than 0.1, are not distinguishable from 0.1 even at the 10% level over most of the subtropics and midlatitudes, but there are some isolated areas such as in the tropical Pacific and the Indian Ocean, where the ratios are close to 0.2 and do differ from 0.1 at the 10% level. Overall, the result that the SST variance ratios are $\ll 1$ indicates that the bulk of the decadal variability in CONTROL is forced by atmospheric noise as opposed to variability internal to the ocean or due to coupled ocean–atmosphere processes not involving the atmospheric or oceanic noise. "Atmospheric noise" in this context includes noise in all of the atmospheric surface fluxes forcing the ocean model, including heat flux, wind stress, and freshwater flux. In those regions where the response is significantly larger than expected from just the direct forcing of the variability by atmospheric noise, there appear to be factors other than atmospheric noise forcing at work, for example coupling between the strength of the noise forcing and biases in the mean state.

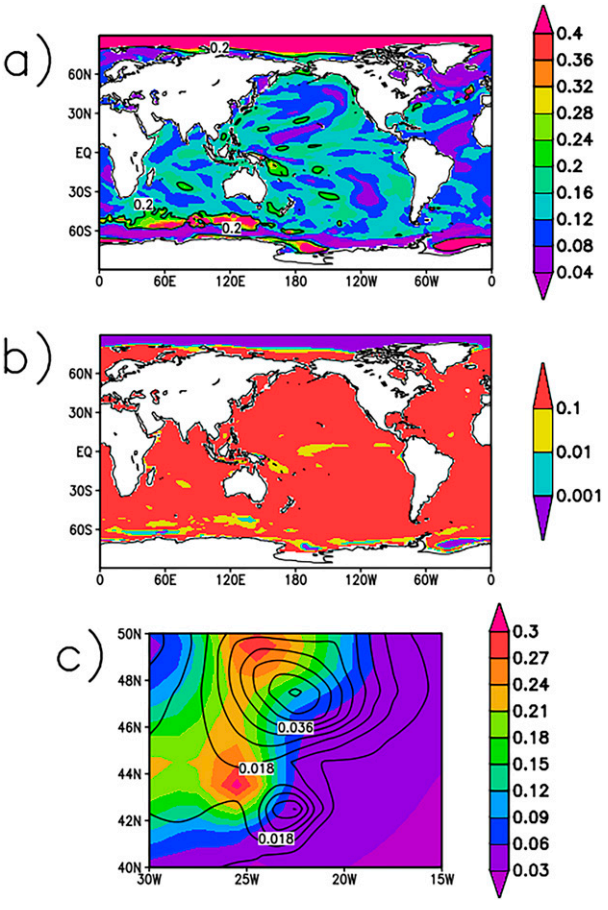

FIG. 3. (a) Ratio of IE to CONTROL variances of decadal SST. A ratio of 0.2 is indicated by a black contour line. (b) F-test significance level that the ratio of 10 times the ratio in (a) differs from 1. Significance levels (%) are 100 times the shaded values and were found from NCL routines equiv_sample_size and ftest. (c) Decadal SST variance (K^2) near 45°N, 22°W for CONTROL (shaded; interval 0.03) and IE (contours; interval 0.006).

It is worth noting that interannual SST variability as given by the variance of the annual mean SST anomalies is also much reduced in IE compared to CONTROL. For example, the IE to CONTROL variance ratio for the SST averaged over the Niño-3.4 region (170°–120°W, 5°S–5°N) is 0.16 for annual means and 0.14 for decadal means. The decadal ratio is not significantly different from 0.1, indicating a response to atmospheric noise forcing. However, the interannual ratio is different from 0.1 at the 1% level, strongly indicating that something besides atmospheric noise is contributing on this time scale.

A small area in the midlatitude North Atlantic (containing "region B" highlighted in Zhang and Kirtman 2019

Brought to you by University of Maryland, McKeldin Library | Unauthenticated | Downloaded 08/23/24 06:34 PM UTC

where the variance ratio test is reported to indicate significant differences) has variance ratio near one, but the significance test fails there due to too few degrees of freedom (white area in Fig. 3b). Figure 3c shows that large variance ratio in this region (essentially a red dot representing a single ocean grid point in Fig. 3a) can be attributed to a small southeastward shift of a strongly spatially concentrated variance pattern in IE relative to CONTROL, with the variance of the pattern about 80% weaker in IE. Comparison with Fig. 2a shows that this shift is associated with a cold bias in IE SST relative to CONTROL. The cause of this anomalous behavior has not been isolated.

The large variance ratios near the North Pole and Antarctica differ from 0.1 at the 0.1% level. These regions are associated with large biases as shown in Fig. 2a.

The influence of the atmospheric noise forcing on the ocean circulation is illustrated by the IE to CONTROL decadal variance ratios for the detrended 9-yr running means of years 201–500 annual mean AMOC streamfunction (Fig. 4a). At all levels above 1000 m, IE AMOC variance is small compared to CONTROL, reaching maximum values of 0.2 to 0.3 near the surface and at deeper levels north of 45°N. However, the ratios are not significantly different from 0.1 at the 10% level, except north of 60°N (Fig. 4b). From the variance ratio, the decadal variability of AMOC-related ocean circulations also appears to be primarily forced by atmospheric noise.

b. *Regional heat budgets of the upper ocean*

The terms in the heat budget [(1a) and (1b)] and their relationship to decadal SST and upper ocean heat content variability for CONTROL and IE are illustrated for two regions with potentially contrasting mechanisms. One is a region in the South Pacific, denoted SPA, and the other is in the northern North Atlantic, denoted NNA. The area of NNA is about 23% of that of SPA. The IE to CONTROL decadal variance ratios for the area mean SST in SPA, NNA, as well as AMV_{mid} (to be discussed in section 4) are small (0.17 in SPA, 0.1 in NNA, 0.1 in AMV_{mid}) demonstrating that the decadal variability in each of the respective SST indices is primarily atmospheric noise forced.

1) SPA REGION

The SPA region is 160°–100°W, 48°–35°S, outlined by the blue box in Fig. 1. Figure 5 shows some overall properties of the SPA decadal ocean temperature and its variability in CONTROL and IE. The area averaged SST anomaly (Fig. 5a) has a period of roughly 30 yr in both CONTROL and IE with typical amplitude of about 0.1°C in CONTROL and less than half of that in IE, with the IE to CONTROL variance ratio 0.17. The vertical structure of the time mean temperature in the top 100 m of CONTROL and IE (Fig. 5b) are similar, but IE is about 0.25°C cooler near the surface increasing to about 0.5°C cooler at 100-m depth. The time–depth diagrams in Figs. 5c and 5d show that the CONTROL and IE anomalies are both confined to the top few hundred meters. CONTROL has a warming trend of about 0.5°C per 300 yr throughout the depth of the ocean, while trends in IE are smaller, with cooling of about 0.1°C per 300 yr below 2000 m. The mechanisms responsible for

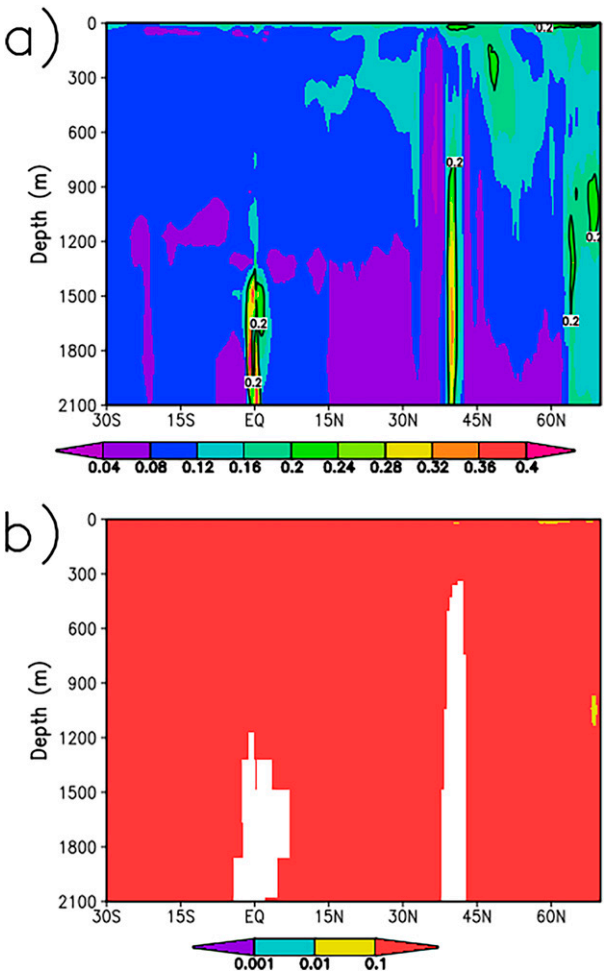

FIG. 4. (a),(b) As in Figs. 3a and 3b, but for the ratio of IE to CONTROL decadal AMOC streamfunction variances. The white areas in (b) have too few degrees of freedom for a significance level to be assigned.

the different mean temperatures near the surface and the stronger trends in the deep ocean have not been determined.

Results from the SPA heat budget diagnosis are shown in Figs. 6a–6d. Quantitative values for the correlations and variance ratios of relationships described in the text are shown in Table 1 (top set of numbers in each row). The full heat content tendency dH/dt and the resolved tendency $D + Q_a$ in [(1a) and (1b)] are shown in Fig. 6a. The resolved tendency has a similar time dependence that of dH/dt and larger variance. The unresolved tendency U (not shown) has similar variance to that of dH/dt, and U damps D. Figure 6b demonstrates that Q_a and D, the two processes that comprise the resolved tendency, approximately cancel. As the variances of both Q_a and Q_O are larger than that of dH/dt, the heat budget (1a) to a rough approximation is an equilibrium balance between net surface heat flux and ocean dynamics:

$$Q_a + Q_O \approx 0. \tag{6}$$

Figure 6c shows that the resolved Ekman contribution D_{ek} to the resolved heat content tendency is a good approximation to

Brought to you by University of Maryland, McKeldin Library | Unauthenticated | Downloaded 08/23/24 06:34 PM UTC

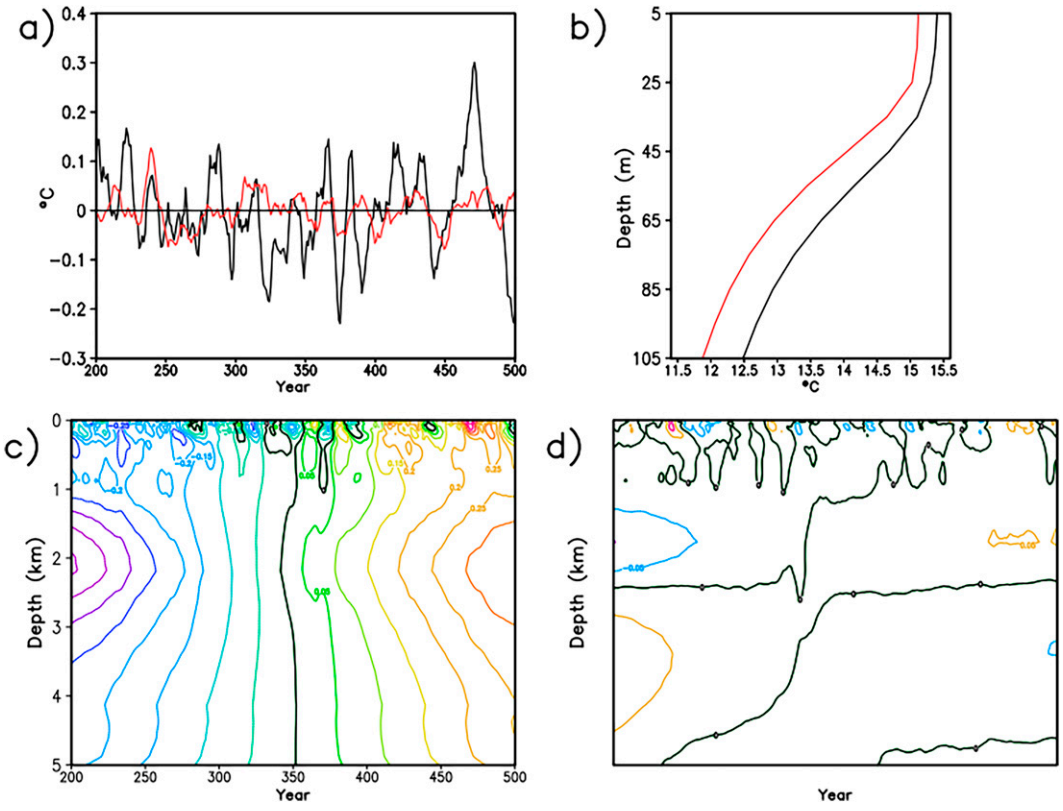

FIG. 5. Decadal ocean temperatures (°C) averaged over area SPA (160°–100°W, 48°–35°S). (a) Detrended SST anomaly for CONTROL (black) and IE (red). (b) Depth distribution of averages over years 201–500 for CONTROL (black) and IE (red). (c),(d) Time-depth distribution of anomalies, not detrended, with contour interval 0.05°C for CONTROL in (c) and IE in (d).

D, indicating that the Ekman transport forced by the resolved wind stress is responsible for the upper ocean heat transport due to the resolved ocean dynamics (also a characteristic of the observed North Atlantic subtropical gyre on seasonal to interannual time scales noted by Buckley et al. 2014). The above descriptions of the CONTROL results in Figs. 1a–1d also apply to the corresponding results for IE in Figs. 1e–1g. Additionally, the ratios of the IE to CONTROL variances for the plotted quantities are all between 0.1 and 0.2, approximately proportional to the ratios of the IE to CONTROL variances expected for the noise forcings. Thus, the results of the heat budget analysis are consistent with decadal SST variability in both IE and CONTROL resulting from forcing by atmospheric noise.

The heat content H is approximately proportional to SST, so that (1a) represents the effects of net surface heat flux and ocean dynamics on SST tendency. The approximate equilibrium heat budget (6), together with the SST correlations and $D \approx D_{\rm ek}$, then seem to suggest that the Ekman response to the resolved atmospheric surface wind stress forces the SPA decadal SST variability, while the atmospheric forcing represented by the net surface heat flux and the unresolved ocean processes both act to damp the heat content and SST anomalies. However, this interpretation turns out to be misleading when the heat budget is represented as the SST response to atmospheric noise and oceanic forcing (see section 4).

As the depth d of the bottom of the region of integration in the heat budget increases, Var(D) and Var(dH/dt) increase. Var(U) decreases from a maximum for d = 10 m (the top layer of the ocean model), decreasing by a factor of 2 for d = 100 m to about Var(Q_a)/3, remaining approximately constant to about d = 1665 m, and then increasing by a factor of 2 to the bottom. The heat content tendency and resolved ocean dynamics contributions are small for d = 10 m and the decadal heat budget is approximately $Q_a + U \approx 0$. As d increases to about 100 m, the magnitude of the resolved dynamics increases and the approximate heat budget becomes $Q_a + U + D = Q_a + Q_o \approx 0$, although Var($dH/dt$) becomes comparable to Var(U) and is not entirely negligible. As d increases to about 500 m, Var(dH/dt) becomes comparable to Var(Q_a), the equilibrium approximation is violated, and the approximate decadal heat budget becomes $dH/dt \approx D + Q_a$.

2) NNA REGION

The NNA region, 20°–36°W, 44°–60°N, is outlined by the red box in Fig. 1. Figure 7 shows overall properties of the NNA decadal ocean temperature and its variability. The area averaged SST anomaly (Fig. 7a) has a dominant period of about 50–70 yr in both CONTROL and IE with typical amplitude of 0.4°–0.5°C in CONTROL and less than 0.2°C in IE, with the IE to CONTROL SST variance ratio of 0.1. The

Brought to you by University of Maryland, McKeldin Library | Unauthenticated | Downloaded 08/23/24 06:34 PM UTC

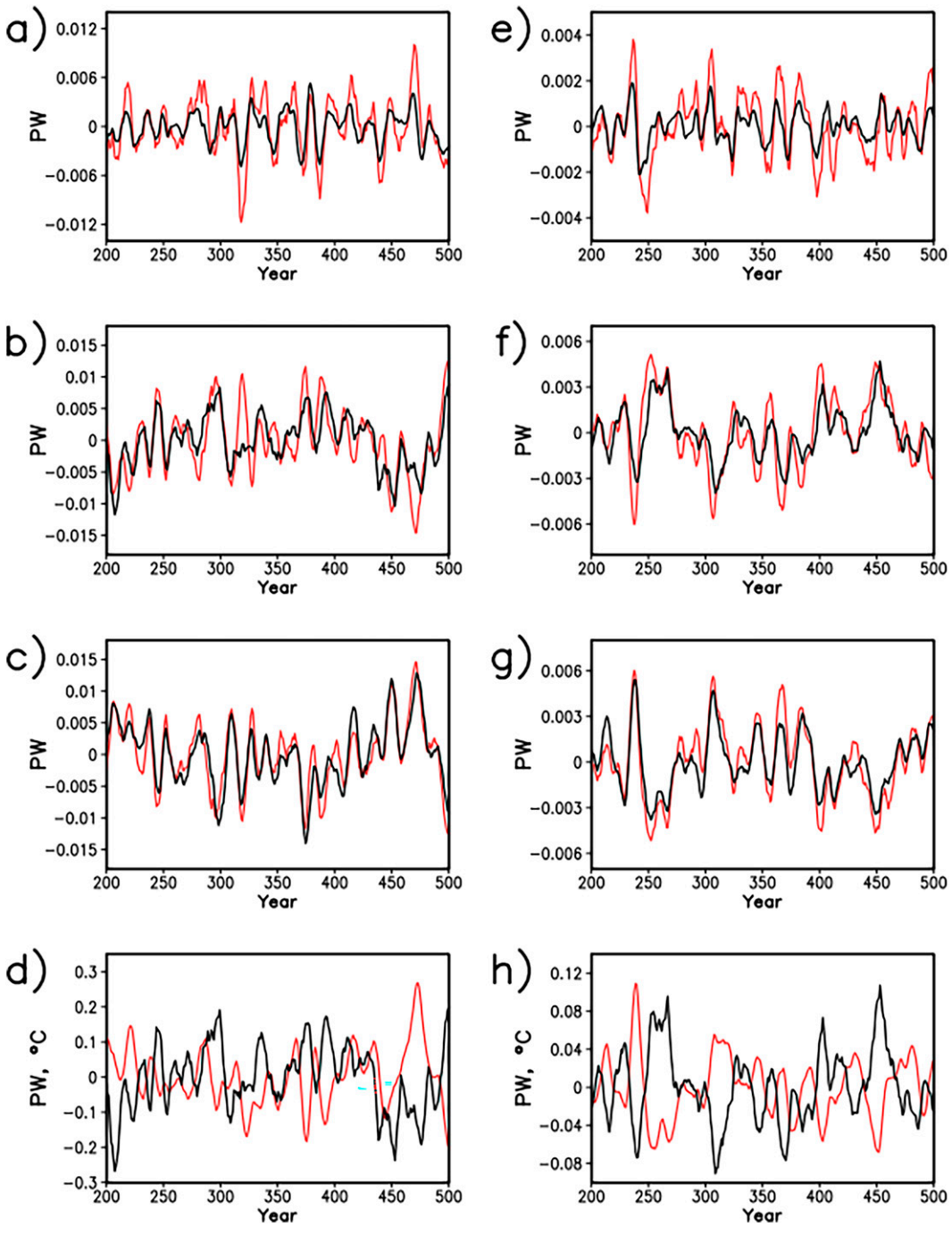

FIG. 6. SPA decadal volume-integrated upper ocean heat budget. The x axes are year; the y axes are PW and also SST (°C) in (d) and (h). (left) CONTROL and (right) IE. (a),(e) Full heat content tendency (dH/dt; black) and total resolved tendency ($Q_a + D$; red). (b),(f) Net surface heat flux (Q_a; black), $-1 \times$ resolved dynamics tendency ($-D$; red). (c),(g) Resolved dynamics tendency (D; red) and Ekman tendency (D_{ek}; black). (d),(h) 23 times the net surface heat flux ($23 \times Q_a$; black), area mean SST (red). Curves are smoothed by a 5-yr running mean.

vertical structure of the time mean temperature in the top 100 m of CONTROL and IE (Fig. 7b) are similar, but IE is about 0.5°C cooler near the surface growing to about 1°C cooler at and below 100 m. The time–depth diagrams in Figs. 7c and 7d show that the CONTROL and IE anomalies are largest in the top 100 m. Vertically coherent anomalies extend to below 2000 m in both CONTROL and IE and propagate downward on decadal time scales. CONTROL has a warming trend of about 0.5°C per 300 yr below 2000 m, while deep ocean trend in IE is cooling of about 0.2°C per 300 yr.

Brought to you by University of Maryland, McKeldin Library | Unauthenticated | Downloaded 08/23/24 06:34 PM UTC

TABLE 1. Correlations and variance ratios between terms of the heat budget [(1a) and (1b)] for CONTROL. Variance ratios (row variable over column variable) are in parentheses. Top numbers in each cell are for SPA and the bottom numbers are for NNA.

	U	D	Q_a	$Q_a + D$	$Q_O = D + U$	H
dH/dt						
SPA	−0.3 (1.4)	0.44 (2.7)	0.09 (4.3)	0.77 (3.1)	0.36 (5.0)	
NNA	−0.6 (21)	0.41 (49)	0.12 (43)	0.71 (29)	0.03 (42)	
U		−0.54		−0.84		
		−0.48 (2.3)		−0.99		
Q_a		−0.75			(0.87)	
		−0.7			(0.99)	
SST	−0.58	0.6	−0.4			0.94
	−0.10	0.83	−0.83			0.98
D_{ek}		0.89 (0.89)				
		0.58 (4.3)				

Results from the CONTROL NNA heat budget diagnosis are shown in Fig. 8, and quantitative values are given in Table 1 (bottom numbers in each row). The resolved tendency is compared to 5 times the full heat content tendency in Fig. 8a. Both time series are similar. The small variance of the heat content tendency and the similarity of the Q_a and Q_o variances indicate that $Q_a + Q_O \approx 0$ is a good approximation to the heat budget, which can also be written as a balance between the unresolved tendency and the resolved tendency, $(Q_a + D) + U = 0$, so that the unresolved and resolved tendencies balance. Var(U) is substantial, about 40% of Var(D). The result that U acts to damp the resolved tendency rather than SST as suggested by Zhang (2017) stands out, but will not be pursued further here. The deep structure of the temperature anomalies shown in Fig. 7b is consistent with U being due primarily to vertical mixing and sharing the resolved tendency over an effective mixing depth of order 500 m. Figure 8b suggests an approximate heat budget $Q_a \cong -D$. Figure 8c shows that the behavior of D_{ek} resembles that of D but that the D_{ek} variance is too small to explain D. Then the geostrophic transport (Buckley et al. 2014) must be important.

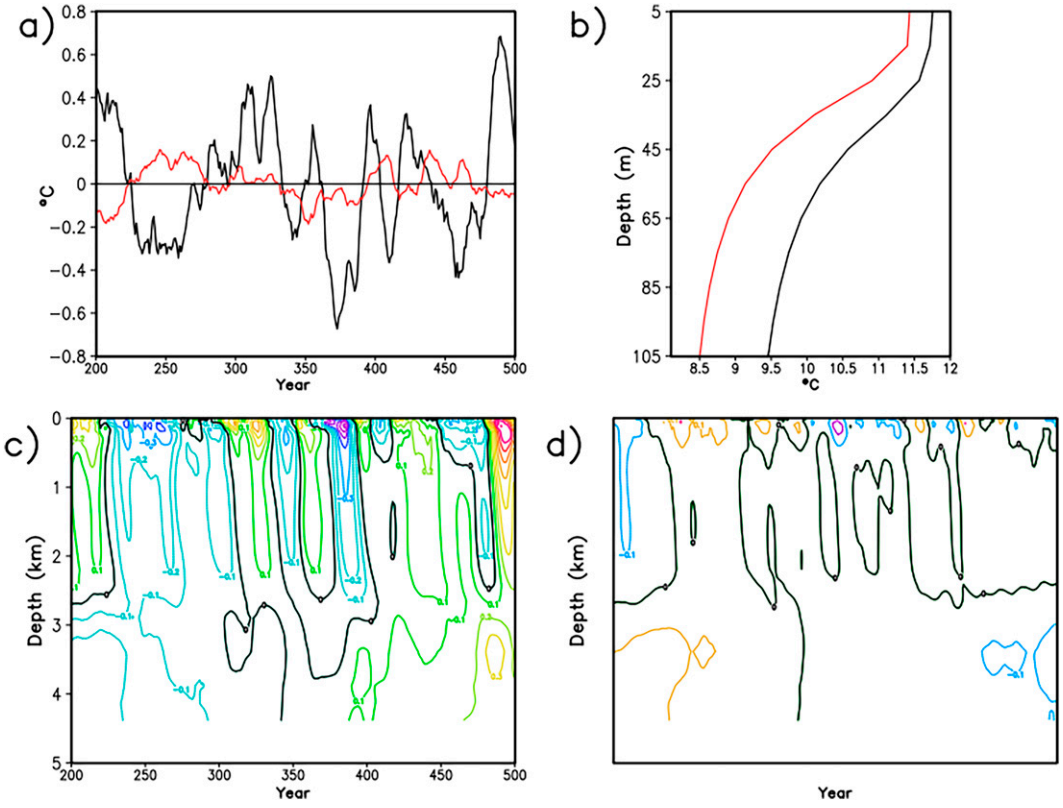

FIG. 7. Decadal ocean temperatures (°C) averaged over region NNA (20°–36°W, 44°–60°N). As in Fig. 5, but for a contour interval of 0.1°C in (c) and (d).

Brought to you by University of Maryland, McKeldin Library | Unauthenticated | Downloaded 08/23/24 06:34 PM UTC

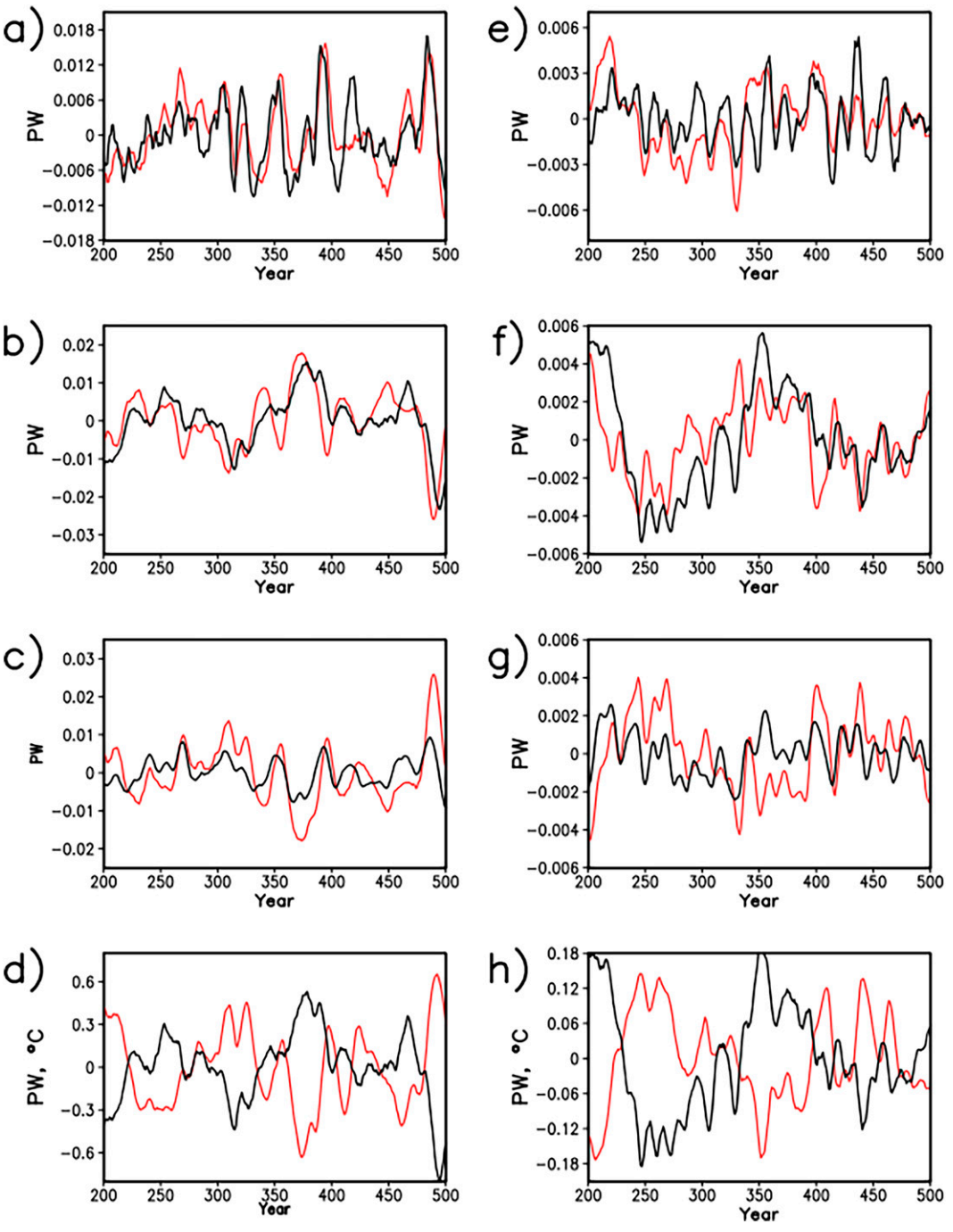

FIG. 8. NNA decadal volume-integrated upper ocean heat budget. As in Fig. 6, but for the multiplicative factors in (a),(e),(d), and (h). (a),(e) 5 times the full heat content tendency ($5 \times dH/dt$; black) and total resolved tendency ($Q_a + D$; red). (b),(f) Net surface heat flux (Q_a; black), $-1 \times$ resolved dynamics tendency ($-D$; red). (c),(g) Resolved dynamics tendency (D; red) and Ekman tendency (D_{ek}; black). (d),(h) 34 times the net surface heat flux ($34 \times Q_a$; black) and area mean SST (red).

The SST is proportional to H. It is apparent from Fig. 8d that SST and Q_a are strongly negatively correlated, so that the net surface heat fluxes appear to act to damp the NNA decadal SST anomaly at all stages of its evolution.

The behavior of the dominant balances in the volume-integrated heat budget as d is increased is qualitatively similar in NNA to that found in SPA. The equilibrium heat budget approximation is not valid for d larger than a few hundred

Brought to you by University of Maryland, McKeldin Library | Unauthenticated | Downloaded 08/23/24 06:34 PM UTC

meters in NNA, consistent with the downward propagation of the anomalies.

The decadal heat budget diagnosis of IE shown in Figs. 8e–8h has similar properties to that of CONTROL, with reduced amplitudes for the various terms. This result is consistent with the SST variability being forced by atmospheric noise surface fluxes, as the oceanic response, SST variability, and atmospheric response to the SST are all qualitatively reduced in proportion to the reduction in the strength of the atmospheric noise surface fluxes.

3) Comparison of SPA and NNA

The decadal SST variability in CONTROL is much stronger in NNA than in SPA, and the associated temperature anomalies extend much deeper below the surface. The heat budget integrated over the top 100 m is an approximate cancellation between the ocean dynamics tendency and the net surface heat flux in both NNA and SPA, and the heat content tendency is proportional to, but smaller than, the resolved tendency. The resolved ocean dynamics tendency in SPA is mostly explained by the Ekman response to the resolved wind stress. The Ekman response is also positively correlated with resolved ocean dynamics tendency in the NNA heat budget, but does not account for the bulk of the ocean dynamics tendency. The deeper penetration of temperature anomalies in NNA than in SPA is related to a stronger reduction of the heat content tendency by the unresolved ocean dynamics relative to the other terms, consistent with deeper and stronger vertical mixing.

The main indications from the heat budget that the role of the ocean dynamics compared to that of the atmospheric heat flux noise might differ in NNA compared to SPA are the reduced role of the Ekman response to the wind stress and the much stronger negative correlation in NNA between Q_a and SST than in SPA.

c. *Ratio of atmospheric surface heat flux noise to net surface heat flux*

An estimate of variance of the heat flux noise in CONTROL is used to address the issue of atmospheric forcing versus ocean dynamics. This estimate is provided from the output of the individual members of the IE atmospheric ensemble as described in section 2d. In the following, the subscript C or superscript C for CONTROL will be understood.

The quantity A_Q is defined as the ratio of the variances of the decadally filtered atmospheric heat flux noise to the net surface heat flux; A_Q is written as

$$A_Q = \frac{\mathrm{Var}(N)}{\mathrm{Var}(Q_a)}. \tag{7}$$

Using the decomposition of $Q_a = F + N$ of (4a) into SST forced F and noise N components, limiting properties of A_Q are:

1) If $A_Q \gg 1$, then $\mathrm{Var}(Q_a) \ll \mathrm{Var}(N)$, so that $|F + N| \ll |N|$ and the noise and SST forced responses approximately cancel. This is a total compensation limit.
2) If $A_Q \ll 1$, then $\mathrm{Var}(F) \gg \mathrm{Var}(N)$. This is the strong SST forcing limit.

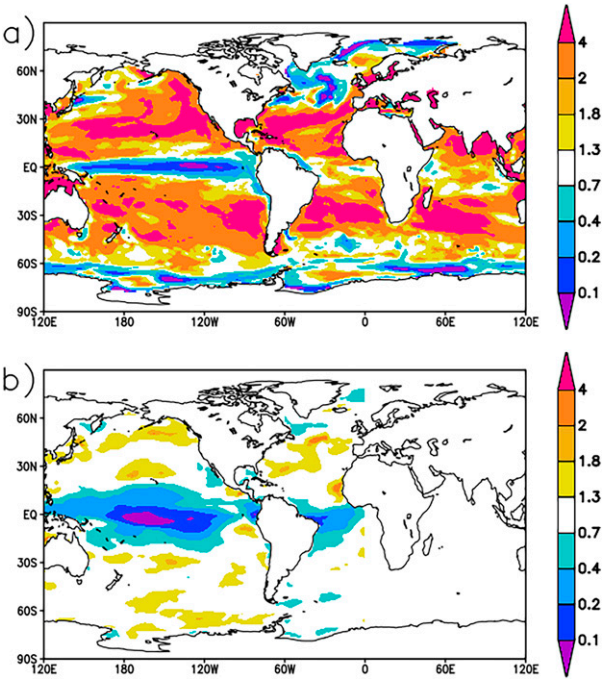

FIG. 9. Variance ratio of mean decadal time-scale noise of IE atmospheric model ensemble members to CONTROL total for (a) net surface heat flux A_Q and (b) surface zonal wind stress A_τ.

3) If $\mathrm{Var}(F) \ll \mathrm{Var}(N)$, then $A_Q \approx 1$. Also, $A_Q \approx 1$ when $2\mathrm{Cov}(F, N) \approx \mathrm{Var}(F)$, which can occur when $\mathrm{Var}(F)/\mathrm{Var}(N) \le 4$. For example, $A_Q = 1$ when $F = -2N$.

To evaluate A_Q, the variance of the noise in CONTROL is taken to be $\mathrm{Var}(N) \approx \mathrm{Var}(N_{\mathrm{IE}})$, where $\mathrm{Var}(N_{\mathrm{IE}})$ is given by (5). This assumes that the noise variances in the atmospheric model members of the IE are about the same as the noise variance in CONTROL. $\mathrm{Var}(Q_a)$ is found from the CONTROL output.

The distribution of A_Q for the surface heat flux is shown in Fig. 9a. There are belts of $A_Q > 2$ between 10° and 40° latitude in both hemispheres and extending across the equator from the north in the Indian Ocean. These are regions where $F + N \approx 0$, a total compensation energy balance relationship between heat flux noise and SST forcing, is approached. That is, the decadal variability is primarily atmospheric heat flux noise forced. The SPA region is heat flux noise forced. There are prominent regions where $A_Q \ll 1$, indicating strong SST forcing of the atmosphere compared to the atmospheric noise. These include regions in the equatorial Pacific, in the northern North Atlantic, including the NNA region, one near the east coast of North America, and one in the North Pacific. Regions where $A_Q \approx 1$ occur in the transitions between total compensation and strong SST forcing regions.

For comparison, the distribution of A_τ, the ratio of atmospheric zonal wind stress noise to total zonal wind stress, defined analogously to (7) but for the decadally filtered wind stress, is shown in Fig. 9b. The SST forced response is strong compared to the noise throughout the low latitudes, particularly in the central equatorial Pacific. Elsewhere $A_\tau \sim 1$

Brought to you by University of Maryland, McKeldin Library | Unauthenticated | Downloaded 08/23/24 06:34 PM UTC

indicating that the magnitude of the SST forced component of the zonal wind stress could be small compared to that of the noise there.

4. Roles of atmospheric surface heat flux noise and ocean dynamics

Next, the question of the influence of the ocean dynamics in the decadal SST variability in CONTROL is examined. While it has been established in section 3 that all decadal SST variability in CONTROL is possibly forced by atmospheric noise, the noise forcing, including heat flux, wind stress, and freshwater flux components, makes contributions to both the surface heat flux Q_a and ocean dynamics Q_O terms in the heat budget (1a). The question will be framed here, following Cane et al. (2017), as a comparison of the CONTROL SST variability with that which would have occurred if the ocean model was a vertically well mixed slab ocean of specified depth ($Q_O = 0$) forced by the CONTROL atmospheric heat flux noise N_C.

Ratio of atmospheric surface heat flux noise to ocean dynamics forcing

Due to the near-equilibrium heat budget $Q_O = -Q_a$ for the decadally averaged upper ocean heat budget (6), A_Q can be written as

$$A_Q = \frac{\mathrm{Var}(N)}{\mathrm{Var}(Q_O)}. \tag{8}$$

From (4a), the heat budget is

$$-F = N + Q_O. \tag{9}$$

That is, the atmospheric heat flux out of the ocean forced by the SST balances the sum of the into-the-ocean atmospheric heat flux noise and ocean dynamics forcings. In the simplified model, to be described in detail in section 4, F is taken to be proportional to SST. Then A_Q turns out to be a direct measure of the relative roles of the atmospheric heat flux noise and ocean dynamics forcings of the atmospheric heat flux response to the SST variability. With this in mind, $A_Q \gg 1$ indicates predominantly atmospheric forcing of SST compared to ocean dynamics forcing, while $A_Q \ll 1$ indicates that SST is forced primarily by ocean dynamics. In regions where $A_Q \approx 1$, the atmospheric and ocean forcings are of similar strength.

The variance ratios for the area averaged atmospheric noise and ocean dynamics forcings, $\overline{A}_Q = \mathrm{Var}(\overline{N})/\mathrm{Var}(\overline{Q}_O)$ with overbar representing area averages, have been computed for the SPA and NNA regions, as well as for the $\mathrm{AMV}_{\mathrm{mid}}$ region (60°–20°W, 40°–55°N) considered by Cane et al. (2017). According to these results, given in the A_Q column of Table 2, the SPA SST is primarily forced by atmospheric heat flux noise, NNA SST primarily by ocean dynamics, while both forcings contribute about equally to forcing the $\mathrm{AMV}_{\mathrm{mid}}$ SST.

A more detailed picture of the roles of the atmospheric heat flux noise and ocean dynamics forcing is obtained here using estimates of the time dependent decadally filtered atmospheric heat flux noise evolution that occurred in CONTROL, together with the ocean dynamics forcing already known from the equilibrium heat budget. The simple model of the equilibrium heat budget of Cane et al. (2017), informed by the A_Q distribution, is used diagnostically to estimate the atmospheric heat flux noise. Then the decadal SST indices in CONTROL in the SPA, NNA, and $\mathrm{AMV}_{\mathrm{mid}}$ regions are decomposed into the parts forced by atmospheric heat flux noise and ocean dynamics. The structures of SST and AMOC variability associated with the atmospheric heat flux noise and ocean dynamics forcings are examined by simultaneous regressions of SST against the decomposed SST indices.

TABLE 2. Variances of T [$\mathrm{Var}(T)$; °C^2], correlations [$\mathrm{Corr}(T, Q_a)$, $\mathrm{Corr}(\tilde{N}, Q_O)$], variance ratios ($A_Q$, A_τ), and λ (W m^{-2} K^{-1}) for the SPA, NNA, and $\mathrm{AMV}_{\mathrm{mid}}$ regions. The ratios A_Q and A_τ use atmospheric noise estimated from IE. The value of λ is chosen so that $\mathscr{A}_Q = A_Q$ using (A7) with $\tilde{N}$ from (A6).

Region	$\mathrm{Var}(T)$	$\mathrm{Corr}(T, Q_a)$	A_Q	λ	$\mathrm{Corr}(\tilde{N}, Q_O)$	A_τ
SPA	0.0085	−0.37	3.4	15	−0.16	1.0
NNA	0.081	−0.8	0.43	14	−0.25	1.1
$\mathrm{AMV}_{\mathrm{mid}}$	0.031	−0.50	1.1	13	−0.43	1.5

The equilibrium heat budget model is described in the appendix. The procedure for estimating the heat flux noise $\tilde{N}$ is described next. In application to CONTROL, the decadally filtered evolution of SST, T, and net surface heat flux Q_a are known. Given the feedback parameter λ, the atmospheric heat flux noise $\tilde{N}$ is evaluated as a residual by removing the feedback from the total heat flux ($\tilde{N} = -F + Q_O$) from (A6) using a trial value λ, and then the value of the estimated variance ratio $\mathscr{A}_Q$ is then determined from (A7). The residual approach to determining the noise evolution has been used previously in Fan and Schneider (2012) with the AMIP ensemble approach, and by Li et al. (2020) with the feedback parameters found using the lag regression approach. Here, the parameter λ is varied until the estimated variance ratio agrees with A_Q found from CONTROL and IE using (7):

$$\mathscr{A}_Q \approx A_Q. \tag{10}$$

The estimate of $\tilde{N}$ using the simple model implicitly includes the contribution to the atmospheric forcing from SST teleconnections, but $\tilde{N}$ will still be referred to as the heat flux noise.

Obtaining a reasonable estimate of λ is the crucial step in this procedure. Estimates of the local atmospheric heat flux feedback to SST using short term lag correlations have found that it can be approximated as a damping of SST (Frankignoul and Hasselmann 1977). Frankignoul et al. (1998) found $\lambda = 20$ W m^{-2} K^{-1} with spatial variations of 50% for the turbulent surface heat flux feedback in observations in the central midlatitude North Atlantic. Frankignoul and Kestenare (2002) reported similar results for the net surface heat flux along with strong annual variations, as did Park et al. (2005). Using a similar approach, Cane et al. (2017) found $\lambda = 13$ W m^{-2} K^{-1} for the $\mathrm{AMV}_{\mathrm{mid}}$ region in the Clement et al. (2015) slab ocean model simulations and $\lambda = 20$ W m^{-2} K^{-1} for a version of the CESM1 CGCM. In a second approach,

Brought to you by University of Maryland, McKeldin Library | Unauthenticated | Downloaded 08/23/24 06:34 PM UTC

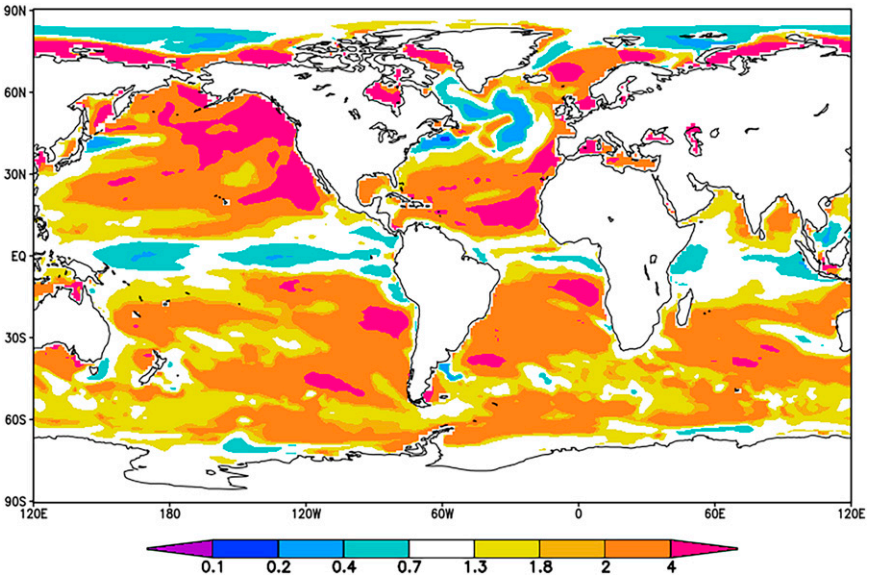

FIG. 10. $\mathscr{A}_Q$, the ratio of decadal time-scale variances of atmospheric net surface heat flux noise from the simple energy balance model to the CONTROL ocean dynamics forcing.

Colfescu and Schneider (2020) used decadal data from an AMIP ensemble using the CAM3 AGCM, an earlier version of the CESM1 atmosphere component to estimate the feedback. This method removes nonlocal effects, and found that the decadal atmospheric response to SST forcing in the North Atlantic generated in an associated CGCM simulation was damping with spatially varying magnitude $\lambda = 10$–30 W m^{-2} K^{-1}. The approach here is to adjust λ to provide a best fit of the ratio of the variances of the area averaged noise to total heat flux, taking the noise variance from the IE and the total from the CGCM. A direct comparison between the results from these three approaches has not yet been made.

The simple model was applied to SPA, NNA, and AMV_{mid} area averages. Table 2 gives variances of the SST indices, estimated heat flux noise, and other regional averages. The values of λ found for the three regions were in the range 13–15 W m^{-2} K^{-1} (Table 2, 4th column). Correlation Corr(T, Q_a) is given for comparison with the values given in Table 1 of Cane et al. (2017). The results for the relative importance of atmospheric and oceanic forcing here (i.e., A_Q) differ from those discussed by Cane et al. (2017) using the same model, in that Cane et al. assume Corr($\tilde{N}$, Q_O) = 0, while Corr($\tilde{N}$, Q_O) $\neq$ 0 results from the solution to (A6) and (10) for $\tilde{N}$. Since the atmospheric noise forces the decadal SST variability in CONTROL, it is reasonable to expect the atmospheric heat flux noise and ocean dynamics forcings to be related. For example, the turbulent surface heat flux in the atmosphere, the Ekman advection, and the strength of the turbulent mixing in the upper ocean are responding to the same noise in the surface wind.

The $\mathscr{A}_Q$ found from (A6) and (A7) with $\lambda = 15$ W m^{-2} K^{-1} and without area averaging is shown in Fig. 10. The pattern is very similar to A_Q in Fig. 9a, although a little weaker in magnitude, indicating that (A6) produces a reasonable approximation to the global distribution of N, even when using a spatially constant λ.

The time dependent decomposition of SST T is given in (A5): $T = T_a + T_O$, where $T_a = \tilde{N}/\lambda$ is the contribution from the atmospheric heat flux noise forcing and $T_O = -Q_a/\lambda$ is the contribution from the ocean dynamics. In the following, this decomposition is applied to the three regions, with T representing the respective SST index. The regressions $R(T)$ of T against SST everywhere and their decompositions are also shown for each averaging region. The decompositions show the relative influences of the atmospheric heat flux noise and ocean dynamics forcing in producing the patterns of SST variability, both inside and outside of the averaging region. The decomposition is

$$R_{\text{SST}}(T) = \text{Reg}(T, \text{SST}) = \frac{\text{Cov}(T_a, \text{SST})}{\text{Var}(T)} + \frac{\text{Cov}(T_O, \text{SST})}{\text{Var}(T)} = \hat{R}_{\text{SST}}(T_a) + \hat{R}_{\text{SST}}(T_O), \tag{11}$$

where Reg(T, SST) is the regression of SST against T, $\hat{R}_{\text{SST}}(T_a)$ is the part of the regression associated with the response to the atmospheric heat flux noise forcing temperature index T_a, and $\hat{R}_{\text{SST}}(T_O)$ is the part associated with the response to the ocean dynamics forcing temperature index T_O.

Figure 11 shows the decomposition obtained for SPA. As indicated in Table 2 and shown in Fig. 11a, this region is forced primarily by the atmospheric heat flux noise, with T_a and T in good agreement and T_O showing smaller variability. The $R_{\text{SST}}(T)$ (Fig. 11b) has a positive maximum over the SPA region and negative values to the northeast and southwest in a horseshoe shaped region in the southeast Pacific/southwest Atlantic/Drake Passage. The negative region is well separated from the SPA region.

Brought to you by University of Maryland, McKeldin Library | Unauthenticated | Downloaded 08/23/24 06:34 PM UTC

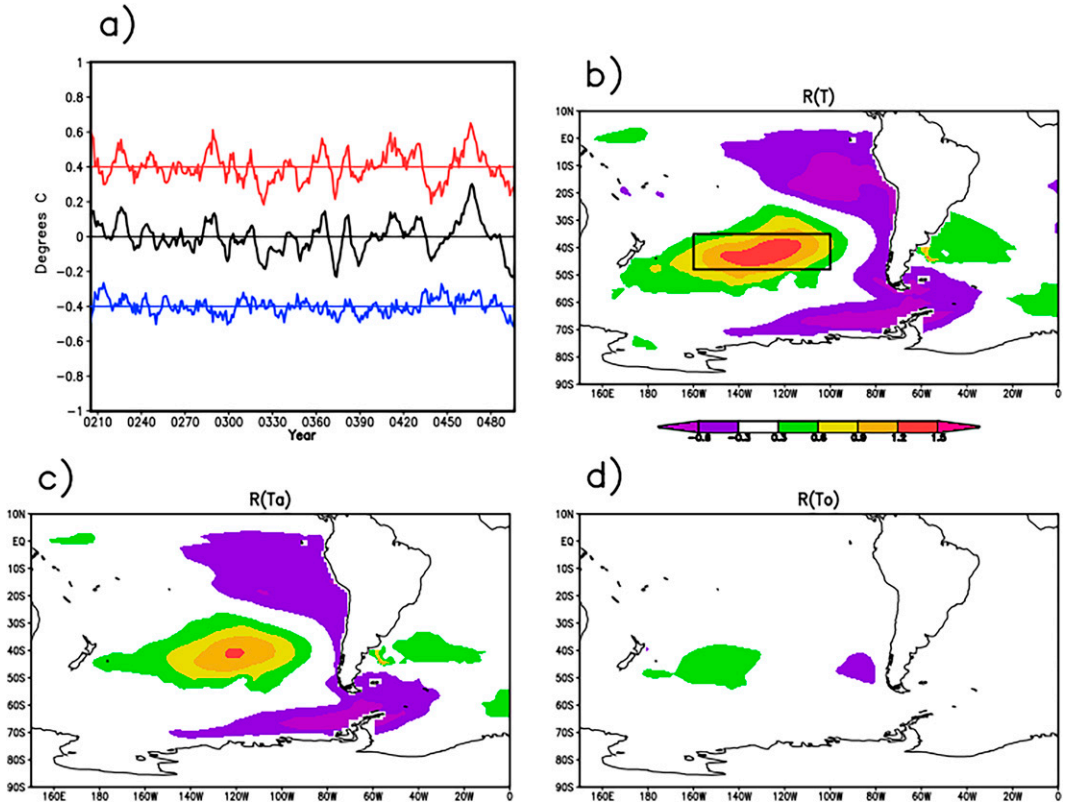

FIG. 11. Decomposition of decadal variability for SPA [black box in (b)]. (a) SST indices (°C): T (black), T_a (red), and T_O (blue). The zero line is shifted up by 0.4°C for T_a and down by 0.4°C for T_O. (b) Regression $R_{\mathrm{SST}}(T)$ of SST against T, (c) contribution $\hat{R}_{\mathrm{SST}}(T_a)$ of atmospheric forcing, and (d) contribution of ocean dynamics forcing $\hat{R}_{\mathrm{SST}}(T_O)$ to $R_{\mathrm{SST}}(T)$ (K K^{-1}).

This bull's-eye/horseshoe structure of $R_{\mathrm{SST}}(T)$ is very similar to the part of the regression due to the atmospheric heat flux noise $\hat{R}_{\mathrm{SST}}(T_a)$, shown in Fig. 11c. The scale of the response to the atmospheric heat flux forcing suggests that the SPA variability is part of a larger scale atmospheric pattern that encompasses much of the eastern South Pacific. The $\hat{R}_{\mathrm{SST}}(T_O)$ part of $R_{\mathrm{SST}}(T)$ due to ocean dynamics forcing (Fig. 11d) has a positive center near the western boundary of SPA, and a negative center near the eastern boundary. This structure could indicate a small westward ocean heat transport through SPA associated with positive SPA T anomalies. Some of the $R_{\mathrm{SST}}(T)$ response in areas remote from SPA may be artifacts of error in the analysis, for example due to error in the equilibrium assumption from the nonnegligible SPA heat content tendency.

The decomposition of the NNA T is shown in Fig. 12a. Since $\mathscr{A}_Q = 0.46$, the variance of the atmospheric heat flux noise forcing is less than half that of the ocean dynamics forcing, and, by the variance measure, the NNA T is primarily forced by ocean dynamics. However, it can be seen from counting peaks of T_a and T_O in Fig. 12a that the atmospheric heat flux noise forcing has a shorter period, about 30 yr, than the ocean dynamics forcing, which has a period of about 100 yr. Despite the larger variance of the ocean dynamics forcing, the influence of the atmospheric heat flux noise forcing on the period of the NNA T is evident, in that the period is about 60 yr, intermediate between the T_a and T_O periods. The positive part of the $R_{\mathrm{SST}}(T)$ extends eastward from the Labrador Sea across the North Atlantic to the Barents Sea, while there is a negative area to the east of the northeast United States to the south of Newfoundland (Fig. 12b). The strongest part of this pattern is a southwest to northeast oriented dipole response to the ocean dynamics forcing $\hat{R}_{\mathrm{SST}}(T_O)$ in the central North Atlantic (Fig. 12d). There is also a projection of the ocean dynamics forcing in the Barents Sea. The $\hat{R}_{\mathrm{SST}}(T_a)$ pattern resembles the $\hat{R}_{\mathrm{SST}}(T_O)$ pattern north of 50°N, but is weaker (Fig. 12c).

The eastern part of the $\mathrm{AMV}_{\mathrm{mid}}$ region contains much of NNA. The $\mathrm{AMV}_{\mathrm{mid}}$ components are shown in Fig. 13a. The variances of T_a and T_O are about equal for $\mathrm{AMV}_{\mathrm{mid}}$ ($\mathscr{A}_Q = 1.2$). However, T_a and T_O are negatively correlated (Table 2), so that $\mathrm{Var}(T) < \mathrm{Var}(T_a) + \mathrm{Var}(T_O)$, although both components contribute positively to the total variance, $\mathrm{Var}(T) > \mathrm{Var}(T_a)$ and $\mathrm{Var}(T) > \mathrm{Var}(T_O)$. As is the case for NNA, the response to the atmospheric heat flux forcing has a multidecadal period, while the time scale of the response to the ocean dynamics is centennial. The $\mathrm{AMV}_{\mathrm{mid}}$ $R_{\mathrm{SST}}(T)$ pattern resembles that of NNA, but with the area of strongest positive response extending westward

Brought to you by University of Maryland, McKeldin Library | Unauthenticated | Downloaded 08/23/24 06:34 PM UTC

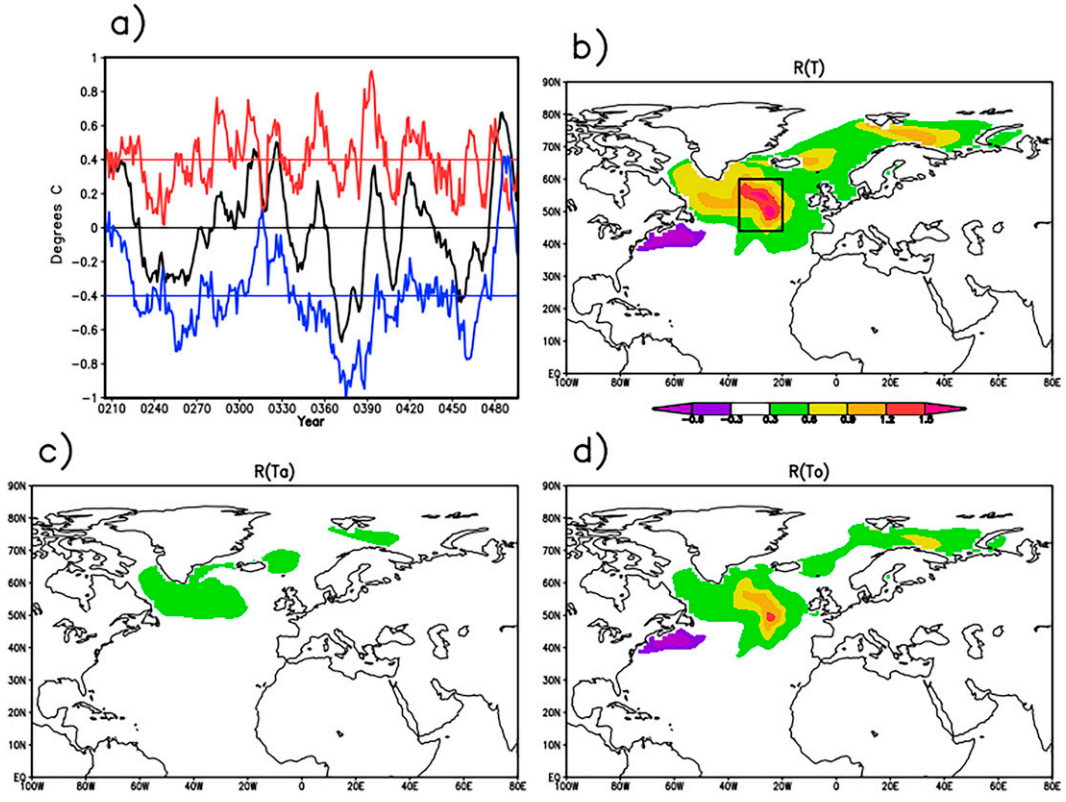

FIG. 12. As in Fig. 11, but for the NNA region [black box in (b)].

into the Labrador Sea and North Atlantic (Fig. 13b). The differences from the NNA pattern in $R_{SST}(T)$ are mainly due to an increase in the atmospheric heat flux noise part $\hat{R}_{SST}(T_a)$ (Fig. 13c). A secondary maximum appears in AMV_{mid} $\hat{R}_{SST}(T_O)$ between Greenland and Canada (Fig. 13d) suggesting additional ocean dynamics forcing occurring in the northwestern part of AMV_{mid} compared to NNA.

Finally, the decomposition of the simultaneous regression of the AMOC streamfunction against the NNA and AMV_{mid} T indices, $R_{AMOC}(T)$ using the approach of (11) is shown in Fig. 14 for the upper 1000 m and from 30° to 60°N. The role of the AMOC in producing the ocean dynamics forcing of T in the index region should be included in the $\hat{R}_{AMOC}(T_O)$ component. If the atmospheric heat flux noise forcing is not influenced by the SST anomalies, $\hat{R}_{AMOC}(T_a)$ could be related to the forcing of the AMOC by the atmospheric noise in the index region. The basic pattern of an increase in the AMOC circulation (positive values) south of about 40°N and a counterclockwise (negative) circulation below 500 m between 40° and 60°N is found in the regression $R_{AMOC}(T)$ and both the $\hat{R}_{AMOC}(T_a)$ and $\hat{R}_{AMOC}(T_O)$ components for both the NNA and AMV_{mid} indices. The size of the response scales qualitatively as the relative variance of the forcing component. The positive near-surface streamfunction is consistent with positive poleward temperature advection in the upper 500 m in $R_{AMOC}(T)$ for NNA up to 45°N, and in the upper 100 m to 60°N (Fig. 14a). The $R_{AMOC}(T)$ for AMV_{mid} (Fig. 14d) shows that the AMOC could be at least partially responsible for Q_O up to 50°N. From comparison of Figs. 14b and 14e, the SST forced by the atmospheric heat flux noise in the western part of the AMV_{mid} region appears to be more strongly related to the AMOC than that in the NNA region since NNA is restricted to the eastern part of AMV_{mid}.

5. Conclusions

Comparison of results from 500-yr current climate simulations made with a CGCM and a 10-atmosphere interactive ensemble version of the same CGCM indicates that most decadal to centennial time-scale SST and AMOC variability in the CGCM outside of high latitudes is forced by internal atmospheric noise. The biases have been reduced in this version of the IE from those in an earlier version. High latitude biases suggest that the IE sea ice coupling strategy should be modified.

Two regions were chosen for analysis of the upper ocean heat budget: SPA in the extratropical South Pacific and NNA in the midlatitude North Atlantic. The upper-ocean heat budget in both regions on these long-time scales is an equilibrium between net surface heat flux and ocean dynamics terms, with heat storage small compared to these components. The details of heat budget by itself do not clearly distinguish between the roles of atmospheric heat flux noise and ocean dynamics forcings.

The IE provides sufficient information to estimate the variance of the atmospheric noise, allowing the overall strength of

Brought to you by University of Maryland, McKeldin Library | Unauthenticated | Downloaded 08/23/24 06:34 PM UTC

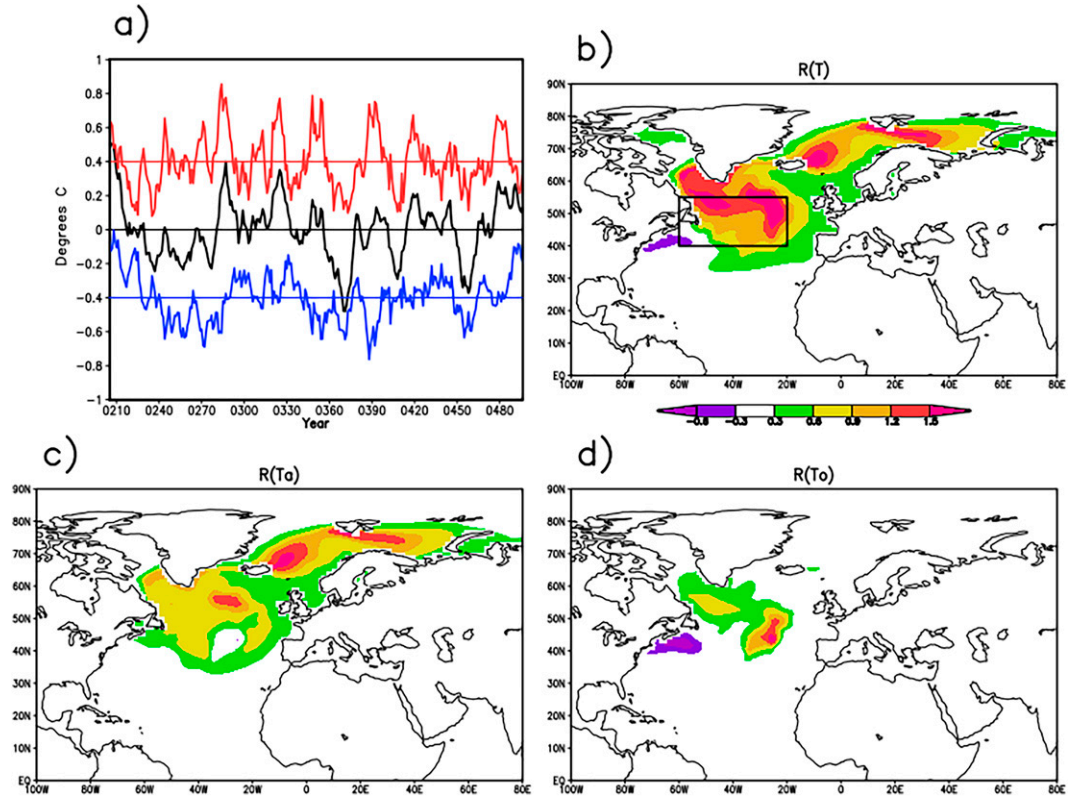

FIG. 13. As in Fig. 11, but for the AMV_{mid} region [black box in (b)].

atmospheric heat flux noise and ocean dynamics forcing in the CGCM heat budget to be compared. The global distribution of the ratio of the variances of the atmospheric heat flux noise to ocean dynamics shows that the atmospheric heat flux noise dominates in the subtropics of both hemisphere and in most of the midlatitude North Pacific. Ocean dynamics is more important in the midlatitude central North Atlantic. Ocean dynamics is also important near 40°N in the western North Pacific and North Atlantic, both regions of strong surface currents, and in the Labrador Sea.

The noise-to-total atmospheric heat flux variance ratio was used to estimate the feedback parameter for the strength of the atmospheric heat flux response to the SST anomalies in CONTROL. In addition to the SPA and NNA indices, results were constructed for the AMV_{mid} index used in Cane et al. (2017). Values of 13–15 W m^{-2} K^{-1} for the feedback parameter produced good fits to the CGCM variance ratio in the three regions, and were used to construct time series for the atmospheric heat flux noise. The responses of the SST to the atmospheric heat flux noise forcing and the ocean dynamics forcing in the index regions were constructed by regression.

For SPA, the atmospheric heat flux noise forcing is large compared to that of the ocean dynamics. The response to the atmospheric forcing explains most of the response to the SPA SST index and is associated with a large-scale pattern with negative SST connections outside the SPA region to the northeast and southeast.

Contrasting behavior was found in NNA, where the ocean dynamics forcing is stronger than the atmospheric heat flux noise forcing. The atmospheric heat flux noise forcing has a multidecadal time scale, while the ocean dynamics forcing has a centennial time scale. The SST response to ocean dynamics forcing explains most of the response to the NNA SST index. Regression of SST against the ocean dynamics forcing includes a positive region inside NNA, and a negative region to the south of Newfoundland, well outside of the forcing region. The negative region, absent in the response to the atmospheric heat flux, suggests that horizontal large scale ocean heat fluxes could be associated with NNA decadal SST variability.

In AMV_{mid}, the strengths of the atmospheric heat flux noise and oceanic forcing are about the same, with a multidecadal time scale for the atmospheric heat flux noise forcing and a centennial time scale for the ocean dynamics forcing. The SST patterns associated with the atmospheric heat flux noise and ocean dynamics forcing components of the AMV_{mid} index have different patterns. In this sense, the AMV_{mid} pattern is composed of two different patterns with differing evolutions. Both patterns broadly resemble the AMV_{mid} pattern (the regression of SST against the AMV_{mid} index) in the index region.

Regression of the AMOC against the NNA and AMV_{mid} indices show similar structures for both the atmospheric heat flux noise and ocean dynamics forcings, with amplitudes

Brought to you by University of Maryland, McKeldin Library | Unauthenticated | Downloaded 08/23/24 06:34 PM UTC

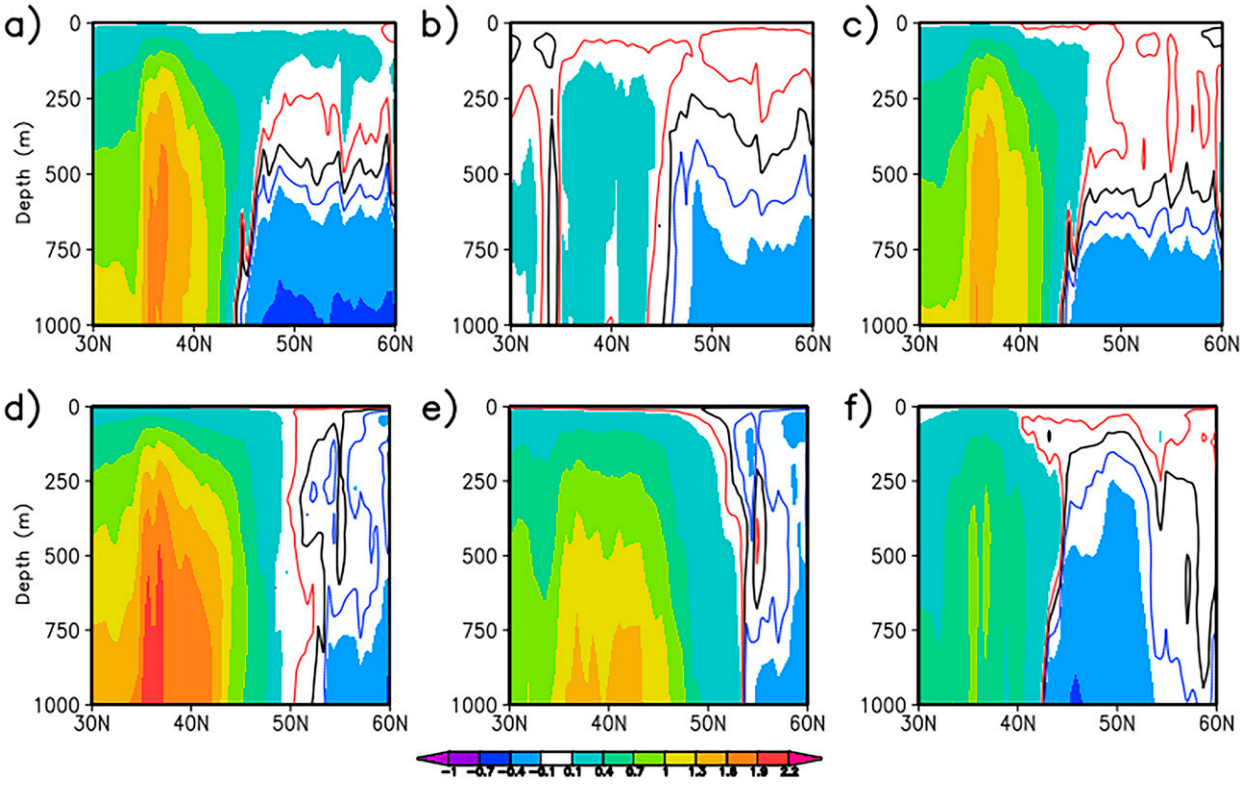

FIG. 14. Decomposition of $R_{\mathrm{AMOC}}(T)$, the regression of the SST index on the AMOC (Sv °C^{-1}) for (top) the NNA index and (bottom) the $\mathrm{AMV}_{\mathrm{mid}}$ index. The quantities are (a),(d) $R_{\mathrm{AMOC}}(T)$; (b),(e) $\hat{R}_{\mathrm{AMOC}}(T_a)$; and (c),(f) $\hat{R}_{\mathrm{AMOC}}(T_O)$ Contours are 0 (black), −0.05 (blue), and 0.05 (red).

approximately proportional to the relative amplitude of the forcing. The AMOC regression against the ocean dynamics forcing can be interpreted as representing the AMOC influence on the SST. The AMOC regression against the atmospheric heat flux noise forcing could represent the forcing of the AMOC by atmospheric heat flux noise.

Our answer to the question of the relative roles of the atmospheric heat flux noise and ocean dynamics forcing of decadal $\mathrm{AMV}_{\mathrm{mid}}$ SST variability in CONTROL is:

1) The strength of the response to both forcings is about the same.
2) The time scale of the part forced by the atmospheric heat flux noise is multidecadal.
3) The time scale of the response to the ocean dynamics is centennial and modulates the part forced by the atmosphere.
4) The shorter time-scale pattern is more apparent in the regression against the $\mathrm{AMV}_{\mathrm{mid}}$ SST index due to its larger scale.

It would be possible to evaluate the contributions of atmospheric heat flux noise and ocean dynamics forcing to decadal SST variability for other models or for analyses of observations by adapting the methods developed here. This could be done without the necessity for the IE diagnosis. The only data needed would be time series of SST and net atmospheric heat flux. The feedback parameter could be obtained from this data either by the lag regression technique or from SST forced AGCM simulations. The ocean dynamics forcing is given by the negative of the atmospheric net heat flux, and the atmospheric heat flux noise is found by removing the atmospheric heat flux response to the SST from the net atmospheric heat flux.

Finally, it is important to note that the calculations described here were made with an eddy parameterized ocean. Several studies have shown that localized air-sea interactions are significantly different in ocean mesoscale resolving simulations (e.g., Bryan et al. 2010; Kirtman et al. 2012, 2017 among many others), and that the ocean internal variability may be much stronger. This raises the question of whether the presence of ocean mesoscale features would alter the conclusions presented here. Moreover, applying the interactive ensemble approach to the ocean component of the CGCM could be used to quantitatively diagnose the role of noise internal to the ocean.

Acknowledgments. EKS acknowledges support from NSF AGS1558821. BK and NP acknowledge the support from NOAA (NA18OAR4310293, NA15OAR4320064, NA20OAR4320472), NSF (OCE1419569, OCE1559151), and DOE (DE-SC0019433). Simulations were made using the facilities of the University of Miami Center for Computational Sciences. Data analysis

Brought to you by University of Maryland, McKeldin Library | Unauthenticated | Downloaded 08/23/24 06:34 PM UTC

and plotting employed the NCL and GrADS software packages. We acknowledge the contributions of Martha Buckley for suggestions on relating heat budget to SST and to include consideration of Ekman heat fluxes. We thank Associate Editor Laure Zanna and three reviewers for their insightful comments.

Data availability statement. The source code for the model used in this study, the NCAR-CCSM4, is freely available at http://www.cesm.ucar.edu/models/ccsm4.0/. The model data are archived at the University of Miami Center for Computational Sciences.

APPENDIX

Simplified Equilibrium Heat Budget Model

The simplified model (Cane et al. 2017) consists of the equilibrium heat budget (6),

$$Q_a + Q_O = 0, \tag{A1}$$

together with the decomposition (4a) of Q_a into SST forced and estimated noise components, F and $\tilde{N}$, respectively,

$$Q_a = F + \tilde{N}, \tag{A2}$$

and the assumption that the SST-forced atmospheric heat flux is represented by local linear damping of T,

$$F = -\lambda T, \tag{A3}$$

where T is the decadally filtered SST and the feedback parameter $\lambda > 0$ gives the strength of the damping of SST by the SST forced atmospheric response. It follows from (A1)–(A3) that

$$\lambda T = \tilde{N} + Q_O = \tilde{N} - Q_a. \tag{A4}$$

Then

$$T = T_a + T_O, \tag{A5}$$

where $T_a = \tilde{N}/\lambda$ is the SST response to the atmospheric heat flux noise and $T_O = Q_O/\lambda = -Q_a/\lambda$ is the response to the ocean dynamics forcing.

Rewriting (A4), $\tilde{N}$ can be calculated for any value of λ, given T and Q_a, from

$$\tilde{N} = \lambda T + Q_a. \tag{A6}$$

The quantity

$$\mathscr{A}_Q = \mathrm{Var}(\tilde{N})/\mathrm{Var}(Q_a) \tag{A7}$$

can then be evaluated.

REFERENCES

Ba, J., N. S. Keenlyside, W. Park, M. Latif, E. Hawkins, and H. Ding, 2013: A mechanism for Atlantic multidecadal variability in the Kiel climate model. *Climate Dyn.*, **41**, 2133–2144, https://doi.org/10.1007/s00382-012-1633-4.

Bombardi, R. J., and Coauthors, 2015: Evaluation of the CFSv2 CMIP5 decadal predictions. *Climate Dyn.*, **44**, 543–557, https://doi.org/10.1007/s00382-014-2360-9.

Bryan, F. O., R. Tomas, J. M. Dennis, D. B. Chelton, N. G. Loeb, and J. L. McClean, 2010: Frontal scale air–sea interaction in high-resolution coupled climate models. *J. Climate*, **23**, 6277–6291, https://doi.org/10.1175/2010JCLI3665.1.

Buckley, M. W., R. M. Ponte, G. Forget, and P. Heimbach, 2014: Low-frequency SST and upper-ocean heat content variability in the North Atlantic. *J. Climate*, **27**, 4996–5018, https://doi.org/10.1175/JCLI-D-13-00316.1.

Cane, M. A., A. C. Clement, L. N. Murphy, and K. Bellomo, 2017: Low-pass filtering, heat flux, and Atlantic multidecadal variability. *J. Climate*, **30**, 7529–7553, https://doi.org/10.1175/JCLI-D-16-0810.1.

Chen, H., E. K. Schneider, B. P. Kirtman, and I. Colfescu, 2013: Evaluation of weather noise and its role in climate model simulations. *J. Climate*, **26**, 3766–3784, https://doi.org/10.1175/JCLI-D-12-00292.1.

——, ——, and Z. Wu, 2016: Mechanisms of internally generated decadal-to-multidecadal variability of SST in the Atlantic Ocean in a coupled GCM. *Climate Dyn.*, **46**, 1517–1546, https://doi.org/10.1007/s00382-015-2660-8.

Clement, A., K. Bellomo, L. N. Murphy, M. A. Cane, T. Mauritsen, G. Rädel, and B. Stevens, 2015: The Atlantic multidecadal oscillation without a role for ocean circulation. *Science*, **350**, 320–324, https://doi.org/10.1126/science.aab3980.

——, M. A. Cane, L. N. Murphy, K. Bellomo, T. Mauritsen, and B. Stevens, 2016: Response to comment on "The Atlantic multidecadal oscillation without a role for ocean circulation." *Science*, **352**, 1527, https://doi.org/10.1126/science.aaf2575.

Colfescu, I., and E. K. Schneider, 2017: Internal atmospheric noise characteristics in 20th century coupled atmosphere-ocean model simulations. *Climate Dyn.*, **49**, 2205–2217, https://doi.org/10.1007/s00382-016-3440-9.

——, and ——, 2020: Decomposition of the Atlantic multidecadal variability in a historical climate simulation. *J. Climate*, **33**, 4229–4254, https://doi.org/10.1175/JCLI-D-18-0180.1.

Danabasoglu, G., S. G. Yeager, Y.-O. Kwon, J. J. Tribbia, A. S. Phillips, and J. W. Hurrell, 2012: Variability of the Atlantic meridional overturning circulation in CCSM4. *J. Climate*, **25**, 5153–5172, https://doi.org/10.1175/JCLI-D-11-00463.1.

Delworth, T. L., and F. Zeng, 2016: The impact of the North Atlantic oscillation on climate through its influence on the Atlantic meridional overturning circulation. *J. Climate*, **29**, 941–962, https://doi.org/10.1175/JCLI-D-15-0396.1.

——, S. Manabe, and R. J. Stouffer, 1993: Interdecadal variations of the thermohaline circulation in a coupled ocean–atmosphere model. *J. Climate*, **6**, 1993–2011, https://doi.org/10.1175/1520-0442(1993)006<1993:IVOTTC>2.0.CO;2.

——, F. Zeng, L. Zhang, R. Zhang, G. A. Vecchi, and X. Yang, 2017: The central role of ocean dynamics in connecting the North Atlantic oscillation to the extratropical component of the Atlantic multidecadal oscillation. *J. Climate*, **30**, 3789–3805, https://doi.org/10.1175/JCLI-D-16-0358.1.

Deser, C., A. Phillips, V. Bourdette, and H. Tang, 2012: Uncertainty in climate change projections: The role of internal variability. *Climate Dyn.*, **38**, 527–546, https://doi.org/10.1007/s00382-010-0977-x.

Dong, B., and R. T. Sutton, 2005: Mechanism of interdecadal thermohaline circulation variability in a coupled ocean–atmosphere

Brought to you by University of Maryland, McKeldin Library | Unauthenticated | Downloaded 08/23/24 06:34 PM UTC

GCM. *J. Climate*, **18**, 1117–1135, https://doi.org/10.1175/JCLI3328.1.

Fan, M., and E. K. Schneider, 2012: Observed decadal North Atlantic tripole SST variability. Part I: Weather noise forcing and coupled response. *J. Atmos. Sci.*, **69**, 35–50, https://doi.org/10.1175/JAS-D-11-018.1.

Frankignoul, C., and K. Hasselmann, 1977: Stochastic climate models. Part II: Application to sea-surface temperature anomalies and thermocline variability. *Tellus*, **29A**, 289–305, https://doi.org/10.3402/tellusa.v29i4.11362.

——, and E. Kestenare, 2002: The surface heat flux feedback. Part I: Estimates from observations in the Atlantic and the North Pacific. *Climate Dyn.*, **19**, 633–647, https://doi.org/10.1007/s00382-002-0252-x.

——, A. Czaja, and B. L'Heveder, 1998: Air–sea feedback in the North Atlantic and surface boundary conditions for ocean models. *J. Climate*, **11**, 2310–2324, https://doi.org/10.1175/1520-0442(1998)011<2310:ASFITN>2.0.CO;2.

Gates, W. L., and Coauthors, 1999: An overview of the results of the Atmospheric Model Intercomparison Project (AMIP I). *Bull. Amer. Meteor. Soc.*, **80**, 29–56, https://doi.org/10.1175/1520-0477(1999)080<0029:AOOTRO>2.0.CO;2.

Gent, P. R., and Coauthors, 2011: The Community Climate System Model version 4. *J. Climate*, **24**, 4973–4991, https://doi.org/10.1175/2011JCLI4083.1.

Gulev, S. K., M. Latif, N. Keenlyside, W. Park, and K. P. Koltermann, 2013: North Atlantic Ocean control on surface heat flux on multidecadal timescales. *Nature*, **499**, 464–467, https://doi.org/10.1038/nature12268.

Hasselmann, K., 1976: Stochastic climate models Part I. Theory. *Tellus*, **28**, 473–485, https://doi.org/10.1111/j.2153-3490.1976.tb00696.x.

Keenlyside, N. S., M. Latif, J. Jungclaus, L. Kornblueh, and E. Roeckner, 2008: Advancing decadal-scale climate prediction in the North Atlantic sector. *Nature*, **453**, 84–88, https://doi.org/10.1038/nature06921.

Kim, W. M., S. G. Yeager, and G. Danabasoglu, 2018: Key role of internal ocean dynamics in Atlantic multidecadal variability during the last half century. *Geophys. Res. Lett.*, **45**, 13 449–13 457, https://doi.org/10.1029/2018GL080474.

——, ——, and ——, 2020: Atlantic multidecadal variability and associated climate impacts initiated by ocean thermohaline dynamics. *J. Climate*, **33**, 1317–1334, https://doi.org/10.1175/JCLI-D-19-0530.1.

Kirtman, B. P., and J. Shukla, 2002: Interactive coupled ensemble: A new coupling strategy for CGCMs. *Geophys. Res. Lett.*, **29**, 1367, https://doi.org/10.1029/2002GL014834.

——, D. M. Straus, D. Min, E. K. Schneider, and L. Siqueira, 2009: Toward linking weather and climate in the interactive ensemble NCAR climate model. *Geophys. Res. Lett.*, **36**, L13705, https://doi.org/10.1029/2009GL038389.

——, E. K. Schneider, D. M. Straus, D. Min, and R. Burgman, 2011: How weather impacts the forced climate response. *Climate Dyn.*, **37**, 2389–2416, https://doi.org/10.1007/s00382-011-1084-3.

——, and Coauthors, 2012: Impact of ocean model resolution on CCSM climate simulations. *Climate Dyn.*, **39**, 1303–1328, https://doi.org/10.1007/s00382-012-1500-3.

——, and Coauthors, 2013: Near-term climate change: Projections and predictability. *Climate Change 2013: The Physical Science Basis*, T. F. Stocker et al., Eds., Cambridge University Press, 953–1028.

——, N. Perlin, and L. Siqueira, 2017: Ocean eddies and climate predictability. *Chaos*, **27**, 126902, https://doi.org/10.1063/1.4990034.

Li, L., M. S. Lozier, and M. W. Buckley, 2020: An investigation of the ocean's role in Atlantic multidecadal variability. *J. Climate*, **33**, 3019–3035, https://doi.org/10.1175/JCLI-D-19-0236.1.

Liu, Z., P. Gu, and T. L. Delworth, 2023: Strong red noise ocean forcing on Atlantic multidecadal variability assessed from surface heat flux: Theory and application. *J. Climate*, **36**, 55–80, https://doi.org/10.1175/JCLI-D-22-0063.1.

Lorenz, E. N., 1963: Deterministic nonperiodic flow. *J. Atmos. Sci.*, **20**, 130–141, https://doi.org/10.1175/1520-0469(1963)020<0130:DNF>2.0.CO;2.

Meehl, G. A., and Coauthors, 2014: Decadal climate prediction: An update from the trenches. *Bull. Amer. Meteor. Soc.*, **95**, 243–267, https://doi.org/10.1175/BAMS-D-12-00241.1.

Milinski, S., N. Maher, and D. Olonscheck, 2020: How large does a large ensemble need to be? *Earth Syst. Dyn.*, **11**, 885–901, https://doi.org/10.5194/esd-11-885-2020.

O'Reilly, C. H., M. Huber, T. Woollings, and L. Zanna, 2016: The signature of low-frequency oceanic forcing in the Atlantic multidecadal oscillation. *Geophys. Res. Lett.*, **43**, 2810–2818, https://doi.org/10.1002/2016GL067925.

Park, S., C. Deser, and M. A. Alexander, 2005: Estimation of the surface heat flux response to sea surface temperature anomalies over the global oceans. *J. Climate*, **18**, 4582–4599, https://doi.org/10.1175/JCLI3521.1.

Schneider, E. K., and M. Fan, 2007: Weather noise forcing of surface climate variability. *J. Atmos. Sci.*, **64**, 3265–3280, https://doi.org/10.1175/JAS4026.1.

Smith, D. M., A. A. Scaife, and B. P. Kirtman, 2012: What is the current state of scientific knowledge with regard to seasonal and decadal forecasting? *Environ. Res. Lett.*, **7**, 015602, https://doi.org/10.1088/1748-9326/7/1/015602.

Wu, Z., E. K. Schneider, and B. P. Kirtman, 2004: Causes of low frequency North Atlantic SST variability in a coupled GCM. *Geophys. Res. Lett.*, **31**, L09210, https://doi.org/10.1029/2004GL019548.

Zhang, R., 2017: On the persistence and coherence of subpolar sea surface temperature and salinity anomalies associated with the Atlantic multidecadal variability. *Geophys. Res. Lett.*, **44**, 7865–7875, https://doi.org/10.1002/2017GL074342.

——, R. Sutton, G. Danabasoglu, T. L. Delworth, W. M. Kim, J. Robson, and S. G. Yeager, 2016: Comment on "The Atlantic multidecadal oscillation without a role for ocean circulation." *Science*, **352**, 1527, https://doi.org/10.1126/science.aaf1660.

Zhang, W., and B. Kirtman, 2019: Estimates of decadal climate predictability from an interactive ensemble model. *Geophys. Res. Lett.*, **46**, 3387–3397, https://doi.org/10.1029/2018GL081307.

Brought to you by University of Maryland, McKeldin Library | Unauthenticated | Downloaded 08/23/24 06:34 PM UTC